Volume 10 | Number 9 | September 2018 | Pages 1173–1350

Metallomics

rsc.li/metallomics

ISSN 1756-591X

ROYAL SOCIETY OF CHEMISTRY

PAPER
Philip A. Doble and George L. Gabor Miklos
Distributions of manganese in diverse human cancers provide insights into tumour radioresistance

Indexed in Medline!

Metallomics

PAPER

View Article Online
View Journal | View Issue

Cite this: *Metallomics*, 2018, **10**, 1191

Distributions of manganese in diverse human cancers provide insights into tumour radioresistance†

Philip A. Doble [a] and George L. Gabor Miklos *[b]

Many cancers are variably resistant to radiation treatment: some patients die within months, while others with the same tumour type and equivalent radiation protocol, survive for years. To determine why some tumours are radiosensitive, while others return after radiotherapy, requires new non-traditional approaches to oncology. Herein we used laser ablation-inductively coupled plasma-mass spectrometry (LA-ICP-MS) to test the hypothesis that Mn functions as a metabolic radioprotector and is an apex predictor of tumour radioresponsiveness. The genesis of this hypothesis lies in microbial and *in vitro* chemical systems. We measured the levels and spatial distributions of Mn in tissue sections of 7 specifically chosen tumour types with distinct clinically documented radioresponsiveness and patient outcomes, namely testis, lung, brain, skin, mesothelium, prostate and breast. Mn levels varied nearly 60-fold between individual tumours, from 0.02 μg g^{-1} to 1.15 μg g^{-1}. The most radiosensitive cancer type, (testis), had the lowest Mn levels and the highest patient survival. Tumours at the radioresistant extreme (glioblastomas and melanomas) had the highest Mn levels and lowest patient survival. A direct association was found between total Mn contents and their variation, and clinically-inferred radioresponsiveness in each of these 7 tumour types, while no such association existed with Cu, Zn or Fe. The LA-ICP-MS data provided unique patient-specific 2D maps of the spatial metallomic heterogeneity of cancer cells and their stroma. These maps have fundamental and far reaching clinical implications. For the first time, Mn-based tumour data may allow for more precise radiodosages and improved treatment for the individual patient.

Received 16th May 2018,
Accepted 12th July 2018

DOI: 10.1039/c8mt00110c

rsc.li/metallomics

Significance to metallomics

Although more than 60% of cancer patients receive radiation treatment, the underlying biological mechanisms of the widespread radioresistance of many human tumours remain elusive despite decades of research. Research efforts have largely focussed on the genomics/proteomics-based enzymology of DNA repair and/or free radical scavenging enzymes such as the superoxide dismutases. Here, we propose the novel hypothesis that tumour radioresistance is predominantly underpinned by non-enzymatic complexes of manganese with small molecular metabolites. These complexes are pivotal to radioprotection. We found that the distributions of manganese in tumours from testis, brain, melanoma, prostate, breast, mesothelium and lung were associated with clinically-inferred radioresistance. No associated were found with other biologically important metals. These findings have very significant implications both for Mn-based mechanisms of radioresistance and patient treatment. For the first time, it may be possible to personalise radiation treatment to an individual patient by measuring the level of manganese in their tumour biopsies.

Introduction

Of the four major pillars of current cancer treatment, namely surgery, chemotherapy, radiation and immunotherapy, it is ionising radiation treatment that alone or in combination with these modalities, underpins ~40% of all cancer cures. Advances in radiation treatment have largely been achieved by improvements in tumour imaging, advanced computation and instrumentation.[1] However, even with the most sophisticated technologies, such as proton beam machines and new brachytherapies, these advances are now near a ceiling. The molecular focus in radiation treatment remains on developing gene expression and proteomic assays to fine tune radiation dosages.[2,3] This is proving challenging. No clinically approved tests have yet revealed where a specific tumour, independently of cancer type, lies on a radioresistance – radiosensitive spectrum at its time of biopsy.

[a] *Elemental Bio-imaging Facility, University of Technology Sydney, Broadway, New South Wales, 2007, Australia. E-mail: Philip.Doble@uts.edu.au*
[b] *Atomic Oncology Pty Ltd, Newport Beach, NSW, 2106, Australia. E-mail: george.miklos@atomiconcology.com*

† Electronic supplementary information (ESI) available. See DOI: 10.1039/c8mt00110c

The problem in a nutshell is that with the exception of inherited radiation-sensitising mutations in a small number of genes, such as Ataxia Telangiectasia Mutated (ATM), no conventional radiotherapeutic indicators are tumour type-agnostic. Given this situation, it is prudent to search for the underlying principles of radiation tumour biology in a different therapeutic area.[4]

One area which holds promise for clinical radiotherapeutics is non-enzymatic metallomics. Here it is known that Mn-complexes render cells variably resistant to the products of ionising radiation by scavenging the main reactive oxygen species (ROS), formed after radiation, namely the superoxide radical $O_2^{\bullet -}$, hydrogen peroxide H_2O_2 and the hydroxyl radical $HO^{\bullet}$. Since the genesis of this Mn-complexes/ROS scavenging area is in non-enzymatic *in vitro* chemistry, and not in conventional enzymology or genomics, it has not yet attracted the attention of the clinical radiology community.

The seminal observation by Gregory and Fridovich[5] in 1974, that a free-living organism lacking detectable superoxide dismutase activity could efficiently scavenge the superoxide radical, $O_2^{\bullet -}$, opened a new vista into the non-enzymatic mechanisms of ROS metabolism. This work led to the finding that the scavenging of $O_2^{\bullet -}$ was achieved by having millimolar concentrations of Mn^{2+} within the cell and it was this dialyzable Mn^{2+} bound to low molecular weight molecules that was the active non-enzymatic scavenger of $O_2^{\bullet -}$.[6] Subsequent *in vitro* cell-free assays revealed that Mn^{2+} formed complexes with organic acids such as malate, pyruvate, propionate, succinate and lactate, and these Mn^{2+} complexes were highly active in scavenging $O_2^{\bullet -}$, the most efficient being Mn^{2+}-lactate.[7]

However, it was not just $O_2^{\bullet -}$ that could be non-enzymatically scavenged by Mn^{2+} bound to low molecular weight molecules. *In vitro* cell free assays revealed the catalase-like activity of Mn^{2+} in bicarbonate buffer.[8] Decomposition of H_2O_2 occurred *via* a Mn^{2+}/amino acid/HCO_3^- complex.[9] This meant that under physiological conditions, the size of the amino acid pool became a critical component of protecting proteins and lipids from oxidative damage.[10] Furthermore, manganous phosphate and manganous carbonate removed $O_2^{\bullet -}$ from solution at rates that were similar to enzymatic removal by superoxide dismutases.[11]

The non-enzymatic mechanisms involving ROS scavenging were clarified in cellular studies, predominantly in microorganisms. It was found that most cellular Mn^{2+} existed as complexes with normal metabolites such as peptides, amino acids, orthophosphates, nucleosides, carbonates and organic acids and their non-enzymatic activities were the dominant processes by which radioresistance was attained. The enzymatic activities of superoxide dismutase, catalase and glutathione peroxidase were minor contributors.[12–19]

We pursued this metabolic area in the context of human tumours because we reasoned that the fundamental properties of Mn, with its 5 unpaired electrons in its 3d orbital, and its conserved chemistry of interactions, should apply to human cancers. We therefore undertook an analysis of patient samples from different human tumour types where clinically-inferred radioresistance had been examined (Table 1), with the aim of using LA-ICP-MS to determine if measurements of Mn levels in tumours could be helpful in the radiation treatment of cancer patients.

Table 1 Clinically-inferred resistance and patient survival after radiation treatment in different categories of cancers. In current patient protocols, radiation treatment may be preceded by surgery, chemotherapy, immunotherapy and adjuvant drugs, or may be used following these interventions. We use radioresistant and radiosensitive only as convenient descriptors. Radioresponsiveness is a continuous variable

Broad tumour category	Clinically-inferred radiation responsiveness	Patient survival after radiation treatment
Brain	Radioresistant	Low
Testis	Radiosensitive	High
Melanoma	Radioresistant	Intermediate and variable
Mesothelioma	Radioresistant	Low
Breast	Variably radiosensitive	High if tumour is localised
Prostate	Variably radiosensitive	High if tumour is localised
Small cell lung	Initially radiosensitive	Low

We assumed that since 95% of cellular Mn^{2+} exists as low molecular weight Mn^{2+} complexes not bound to enzymes, then total cellular Mn content in tumours could be a useful initial assay for examining clinically-inferred radioresistance. We deemed it likely that total Mn content in tumours would be a reasonable proxy of Mn^{2+} in high symmetry complexes, which are the strongest indicator of radioresistance to date.[19] Since the other key components of Mn^{2+}-complexes, namely the cellular pools of peptides, nucleosides and free amino acids, are generally present at millimolar concentrations in normal cells, we assume that they are in similar concentrations in tumour cell populations. There is certainly likely to be a large and diverse pool of peptides, since there is no shortage of dying cells and their autoproteolytic digests within most solid tumours. The large necrotic areas in many cancers attest to this consequence.

We hypothesise that: (i) some cells in human tumours will have accumulated sufficient Mn to be protected from radiation-induced ROS damage at a given radiation dosage, and (ii) the differences in Mn levels within a tumour will be visible in 2D analyses of tissue sections and provide information of clinical utility to patient treatment.

To test the above inferences on Mn-based radioresistance, we utilised LA-ICP-MS instrumentation to go directly from standard human pathological sample material to data analysis, with no interposed sample manipulation steps. The outputs were 2D maps that revealed a patient-specific, Mn-based, metallomic cartography of cancer cells embedded in their supporting stroma. The metallomic topography of such maps allowed testable inferences to be drawn on the probabilities of tumour radioresistance and reoccurrence for that specific tumour.

Experimental

Pathological material: tissue microarrays

Arrays were purchased from US Biomax (www.usbiomax.com) and contained de-identified patient tumour cores designated as follows; ME804a, primary and metastatic melanomas; TE802, testicular seminomas and lymphomas; GL806c, glioblastomas; LC802a, small cell lung cancers; MS801a, mesotheliomas; BR804a,

breast cancers and breast adjacent tissue; PR806, prostate and prostate adjacent tissue; and FDA999f, different normal tissues. H&E stained slides were scanned at Royal College of Pathologists of Australasia Quality Assurance Programs (RCPAQAP) Pty Limited, St Leonards NSW 2065, Australia, rcpaqap@rcpaqap.com.au and images examined *via* ImageScope software from Aperio. The analyses of the tissue microarrays were executed under the University of Technology Sydney ethics approval UTS HREC 2010-481.

Laser ablation-inductively coupled plasma-mass spectrometry

The elemental images were acquired on an Agilent 7770 ICP-MS coupled to a New Wave Research NWR193 ArF excimer laser. The ICP-MS was fitted with 's' lenses to enhance sensitivity. High purity liquid argon (Ar) was used as the carrier gas and plasma source, while ultra-high purity (99.999%) hydrogen (H_2) was used as the reaction gas. The LA-ICP-MS system was tuned on a daily basis and for both standard mode and reaction mode using NIST 612 Trace Elements in Glass for maximum sensitivity and to ensure low oxide formation. Low oxide production was assured by measuring a mass-to-charge ratio (m/z) of 248/232 (representing $^{232}Th^{16}O^{+}/^{232}Th^{+}$) and was consistently less than 0.3%. The instrument was fine-tuned for tissue analysis using matrix-matched tissue standards with monitored mass/charge ratios (m/z), 55 (Mn), 56 (Fe), 63 (Cu) and 66 (Zn). The ICP-MS dwell times were set according to the parameters outlined by Lear *et al.*[20] to ensure the elemental image maintained the dimensions of the specimen.

Operational parameters for ICP-MS

The radio frequency power was 1250 Watts; the cooling gas flow rate was 15.0 litres per minute; the carrier gas flow rate was 1.2 litres per minute, the torch sample depth was 4 millimetres; the quadrupole bias was −3.0 Volts; the octopole bias was −6.0 Volts; the dwell time was 62 milliseconds per m/z; extraction lens 1 was 5.0 Volts; extraction lens 2 was −100.0 Volts and the hydrogen collision gas was 3.1 milliliters per minute.

Laser ablation of pathological material

A glass microscope slide with an unstained section from a tumour sample was placed in an ablation chamber and a 35 micrometer diameter high energy laser beam was focused onto the section and some of the biological material was vaporised as a result of energy transfer from the laser beam. Argon gas carried the resulting particulate matter into the ICP, which at a temperature exceeding 7000 degrees Celsius, but below 10 000 degrees Celsius, atomises and ionises the particulate matter to its constituent elements. The use of collision/reaction[21] minimised spectral interferences, and "removed" polyatomic ions such as and nitrogen:argon ($^{15}N^{40}Ar^{+}$) and oxygen:argon ($^{16}O^{40}Ar^{+}$) species that would otherwise appear as 55 and 56 signals, respectively, and incorrectly attributed to ^{55}Mn and ^{56}Fe. In the dynamic reaction cell, interfering polyatomic ions were converted to a different species at a higher mass : charge ratio (m/z), and no longer interfered with the target ions. Following emergence from the reaction cell, the ions were focused into a quadrupole mass filter where they were separated by their m/z ratios and detected and quantified.

The immediately adjacent tissue section from the H&E slide was de-paraffininised to generate a 2D elemental map. The laser was rastered across a sample from left to right, one track at a time from top to bottom, where the track was 35 micrometers in width. Each track was saved as individual comma separated values (csv) files and combined with an inhouse written python script into a visual toolkit (vtk) format. These files were processed into quantified and background corrected images using Paraview, an open source imaging software package (Kitware Inc. 28 Corporate Drive, Clifton Park, New York, 12065 USA).

Preparation of tissue standards

Matrix matched standards were prepared from chicken breast tissue removed of any fat or connective material and were partially homogenised using an OmniTech TH tissue homogeniser fitted with a polycarbonate probe (Kelly Scientific, North Sydney, New South Wales, Australia), and subsequently spiked with standard Mn, Fe, Cu, and Zn solutions. Solutions were prepared using high purity (min 99.995%) soluble chloride, sulfate, or nitrate metal salts (Sigma-Aldrich, Castle Hill, New South Wales, Australia) dissolved in 1% HNO_3 (Choice Analytical, Thornleigh, New South Wales, Australia) and diluted to concentrations of *ca.* 100 000 micrograms per millilitre and 10 000 micrograms per millilitre. Aliquots of the chicken breast were then spiked with varying concentrations of each of the elements and homogenised at low speed for 5 min. Six *ca.* 250 milligram aliquots of each homogenised tissue standard were digested in 5 : 1 Seastar Baseline grade HNO_3/H_2O_2 (Choice Analytical) in a Milestone MLS 1200 closed vessel microwave digester (Kelly Scientific) and analysed using solution ICP-MS to confirm the concentration and homogeneity of each element in the tissue standards. The spiked tissue was frozen and cut into 30 micrometer sections and placed onto glass microscope slides for analysis.

Calibration and background correction

The prepared matrix-matched tissue standards were used to construct calibration curves for signal normalisation of analytes across 6 concentration levels. Each standard was analysed by LA-ICP-MS under the same parameters as the tissue microarrays as described earlier. 7 consecutive 10 second raster lines were acquired for each level of standard from which the average signal was calculated and plotted against concentration. To aid simple interpretation of the quantified metallomic images, a normalisation procedure was used to compare each acquisition, reported in units of normalised counts per second (npcs). Here, we divided the slope of the calibration curves to generate a correction factor that was applied to each of the images to ensure consistent signal sensitivity throughout the study. The concentrations of the analytes, slopes, correlation coefficients and correction factors are detailed in ESI,† Table S1.

Background corrections were performed on ^{55}Mn, ^{56}Fe, ^{63}Cu and ^{66}Zn by extracting the signal from representative areas of the image where no tissue was ablated. The median signal of the background was subtracted from each individual voxel of the image.

Results

We measured the levels and distributions of Mn, Cu, Zn and Fe in 359 formalin-fixed, paraffin-embedded, unstained tissue sections from tumours of cancer patients and from organs of healthy individuals. The details are in Materials and methods and in Hare *et al.*[22]

Controls and standards from normal tissues

To provide a foundation for the cancer data, we determined metal levels and their variations in tissue sections from the liver, brain, heart muscle, pancreas and spleen of normal individuals. We did so since there are important gene expression data on metal transporters that modulate influx and efflux of Mn from the gastrointestinal tract after dietary ingestion and its release into the bloodstream.[23,24] The amount of Mn available to a tumour, be it at primary or metastatic sites, will initially be determined by how much Mn passes through this gateway into the bloodstream.

Laser ablation was carried out on a standard glass slide on which an unstained section of patient material, derived from a tissue microarray, had been cut at 5 μm thickness from a formalin-fixed paraffin-embedded (FFPE) block. Fig. 1(A) shows an example of a single laser-ablating track in the abscissa (x) direction on a section of normal liver.

A 6 pixel portion of this 30 pixel single laser track has been overlaid with the high quality pathological features of an hematoxylin and eosin (H&E) stained photomicrograph from the tissue section immediately adjacent to the unstained, laser-ablated section in Fig. 1(B).

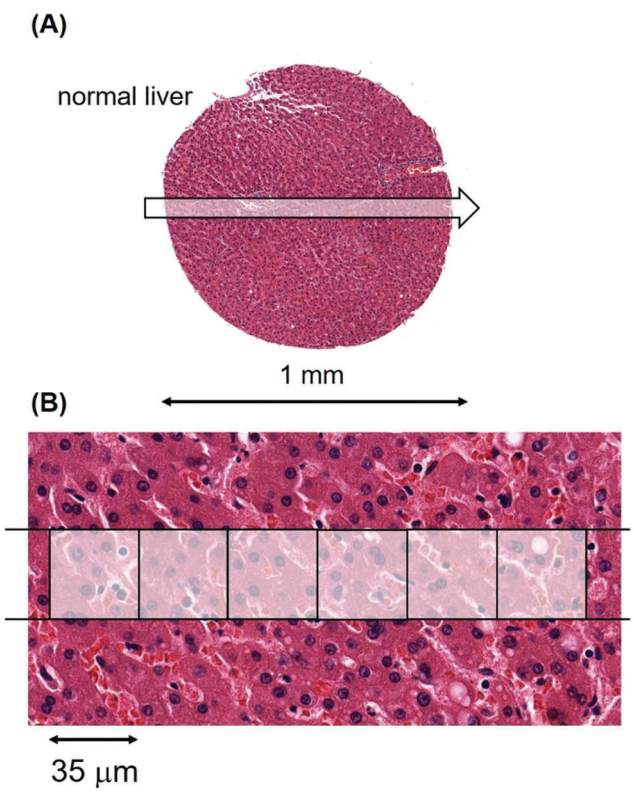

Fig. 1 LA-ICP-MS of a tissue sample from the liver of patient #351, a healthy 38 year-old male. (A) Laser ablation track across the sample. (B) High resolution image of a 6 pixel part of the track where each pixel has dimensions of 35 × 35 μm^2.

Each pixel in the image represents a voxel of 35 × 35 × 5 μm^3. The metallomic data from this single 1 mm track (of length 30 pixels), were acquired in 7.1 seconds.

By laser ablating tracks in the abscissa (x) direction followed by sequential contiguous ablation in the ordinate (y) direction, we generated a Cartesian coordinates system map of quantified metals for the entire liver sample. The median of all voxels in a sampled region represented the median Mn, Cu, Zn and Fe levels of that section for that particular patient. The levels were normalised and corrected for background by concurrently measured controls of precisely defined standards and expressed in units of normalised counts per second (ncps) (Materials and methods and ESI,† Table S1).

The liver tissue sample in Fig. 1 provided ~800 voxels of biological material for evaluation. We analysed data from this entire sample and from smaller regions of the 800 voxel spot to determine the minimum sample size needed to obtain a reliable estimate of metallomic values. In nearly all cases, sample sizes of 150 voxels did not deviate from the median of the whole sample by more than 10%, and usually by less than 5% (ESI,† Table S2). We used a minimum sample size of 150 voxels, usually more, for analyses of normal and cancerous samples, equivalent to sampling between 500 to 1000 cells.

The background-corrected metal contents per voxel in normalised counts per second (ncps) and their associated standard deviations (StDev) for a 500 voxel sample from this healthy liver were; Mn = 16 970 ncps, (StDev 2,820); Cu = 17 660 ncps, (StDev 11 430); Zn = 45 530 ncps, (StDev 5101) and Fe = 4 471 690 ncps, (StDev 1 207 010). These values can equally be expressed as μg g^{-1}, with which the mass spectrometry community is familiar. For the above, these values are; Mn = 0.65 μg g^{-1}; Cu = 6.01 μg g^{-1}; Zn = 9.79 μg g^{-1} and Fe = 249 μg g^{-1}. The broad audiences for these LA-ICP-MS data include oncologists, radiologists, pathologists and genome and proteome specialists, most of whom are more familiar with counts per second terminology. We have therefore used it as the preferred method of presentation.

The quantitative Mn levels in five normal tissues/organs, (liver, cardiac muscle, spleen, pancreas and cerebral cortex), the variation between them, and the variation between different healthy patients, are given in ESI,† Table S3.

We now examine patient samples from each of the seven tumour categories described in Table 1 to evaluate any metallomic linkages to tumour radioresistance. Extensive patient-centric information on each of these tumour types is available from the UpToDate clinical decision support resource for physicians (https://www.uptodate.com/home).

1. Mn, clinically-inferred radioresistance and patient survival in cancers of the testis and the brain. Certain cancer types of the testis (namely, classical seminomas) are clinically accepted as being exquisitely radiosensitive.[25–29] In contrast, advanced brain cancers such as glioblastoma multiforme are notoriously radioresistant.[30,31] These two tumour types represent extremes

of the radiotherapeutic spectrum shown in Table 1 and are a starting point for asking if Mn-based metabolic systems are major contributors to the radioresistance of human tumours.

The metallomic data on median Mn levels from tumours of 53 patients with classical testicular seminomas are compared to data from 26 patients with glioblastomas (Fig. 2(A and B), respectively), and their overall survival curves are shown in Fig. 2(C and D), respectively. As we do not have overall survival data for these 53 classical seminoma patients or for these 26 glioblastoma patients, they have been derived from the US National Cancer Institute's Surveillance, Epidemiology and End Results (SEER) database (http://www.seer.cancer.gov).

The median level of Mn from the tumour of each individual cancer patient is represented as a separate box in the histograms of Fig. 2. The 53 classical testicular seminoma patients clustered around a median Mn tumour level of 1030 ncps per patient, while the brain patients had a more than 3-fold higher median Mn tumour level of 3560 ncps, with some patients exceeding 10 000 ncps. The two distributions differed significantly, (Kolmogorov–Smirnov test, D = 0.83 with a corresponding P = 0.00). Furthermore, 95% of the classical seminoma patients had median Mn tumour levels of $<$2000 ncps, while 81% of the brain patients had Mn tumour levels of $>$2000 ncps. There was a large between-patient variation in the glioblastomas with a standard deviation of 3760, compared to 410 for the seminomas.

We found only one study on Mn in glioblastomas using LA-ICP-MS applied to tissue sections, and it involved three patients.[34] The Mn tumour levels in that study varied 10-fold between two patients, in line with the large variation that we observed between tumours of glioblastoma patients. No information was available on the third patient.

An additional aspect of Mn levels in the tissue sections of the seminomas and glioblastomas is illustrated in Fig. 3. While cell densities are approximately comparable between these two tissue sections, (Fig. 3(B and D)), their median Mn tumour levels are nearly five-fold different at 1000 ncps and 4760 ncps for the seminomas and glioblastomas, respectively. Thus, Mn tumour levels are not, in general, due to cell density differences.

Patient survival. The overall survival data for classical seminomas and glioblastomas are available from three independent sources and the data from those sources are congruent.

First, the SEER database has overall survival data for cancer patients irrespective of their treatment modalities. These data encompass all types of treatment received by patients, such as surgery, radiation and chemotherapy. Patients with testicular seminomas have low cancer-specific mortality, with more than 98% of patients still alive after 5 years.[32] Patients with glioblastomas have a high cancer-specific mortality with less than 3% alive after 5 years[33] (Fig. 2(C and D) respectively).

Second, The Pathology Atlas of the Human Cancer Transcriptome,[35] has survival data for testicular cancers and gliomas irrespective of their treatment modalities, and these survival curves closely mirror those from the SEER database.

The third data source is from those patients for whom radiation was the sole or major treatment. These data match those from the above two sources. Radiation-treated seminoma patients have cure rates exceeding 95% at 10 years leaving little doubt of their extreme radiosensitivity.[25–28] By contrast, radiation treatment of tumours of glioblastoma patients barely prolongs survival, with less than 10% of patients surviving at 3 years, even after radiation to 90 Gy and adjuvant temozolomide treatment.[30,31] The most compelling finding of radioresistance in glioblastomas is

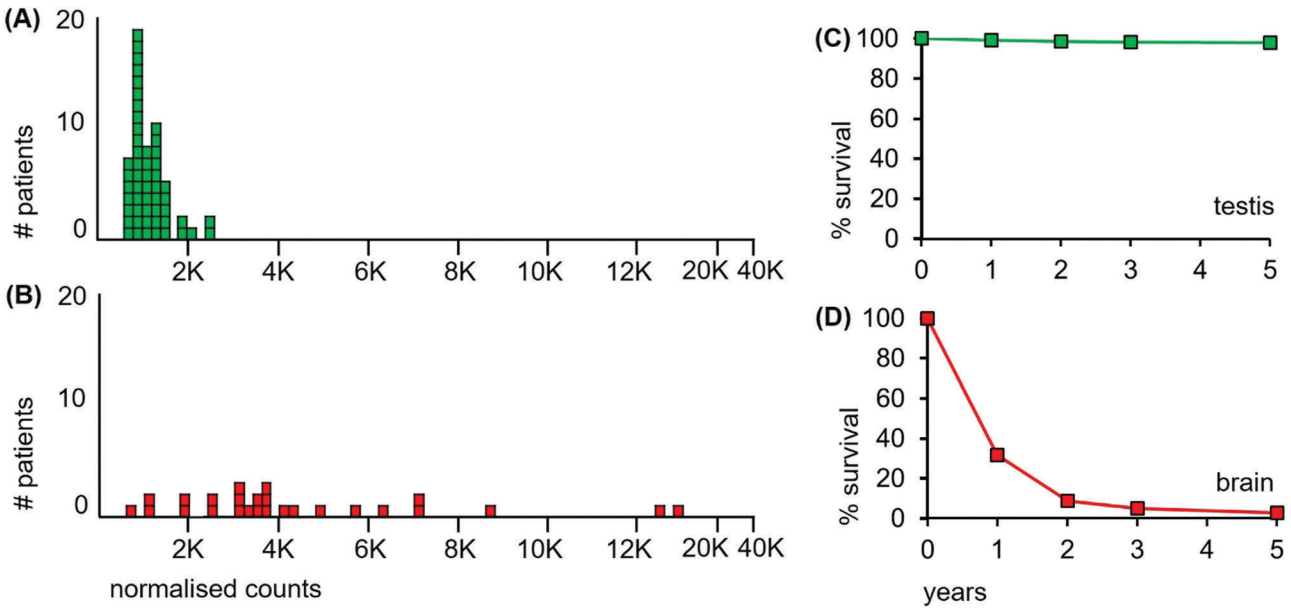

Fig. 2 Median Mn levels in tumour sections from patients with cancers of the testis and of the brain and their survival curves. (A) Mn levels from each of 53 classical seminoma patients (green boxes); (B) 26 glioblastoma patients (red boxes). Overall survival curves over a 5 year period for patients with (C) classical seminomas (estimated from reference[32]); and (D) glioblastomas (estimated from reference[33]).

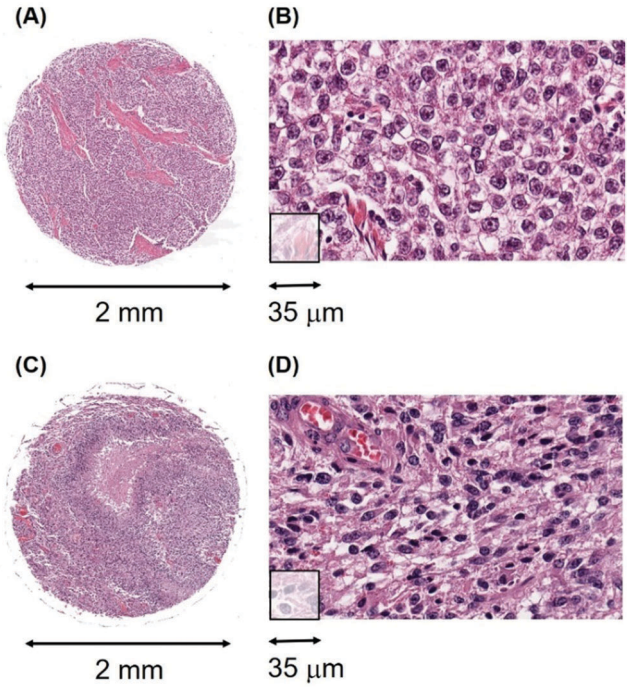

Fig. 3 Generic examples of the morphologies of classical seminoma and glioblastoma. (A and B), low and high-power images from patient #47, a 55 year-old male with a classical seminoma showing characteristic collagen streaks throughout the tumour (pink), (A). (C and D), patient #197, a 40 year-old male with glioblastoma showing characteristic abnormal blood vessels and areas of necrosis, visible as the large pink area in (C).

that tumours reoccur within regions that were given even higher doses of radiotherapy.

Levels of other metals: Zn. The large differences in the median Mn tumour levels of patients with classical seminomas or glioblastomas contrasts markedly with the levels of Zn determined from the same voxels in the same tumours (Fig. 4).

The 53 classical testicular seminoma patients had a median Zn tumour level of 8520 ncps per patient, while the brain patients had a median Zn tumour level of 7740 ncps. The standard deviations were similar at 3490 and 3520, respectively. The two distributions did not differ significantly, (Kolmogorov–Smirnov test, $D = 0.20$ with a corresponding $P = 0.46$).

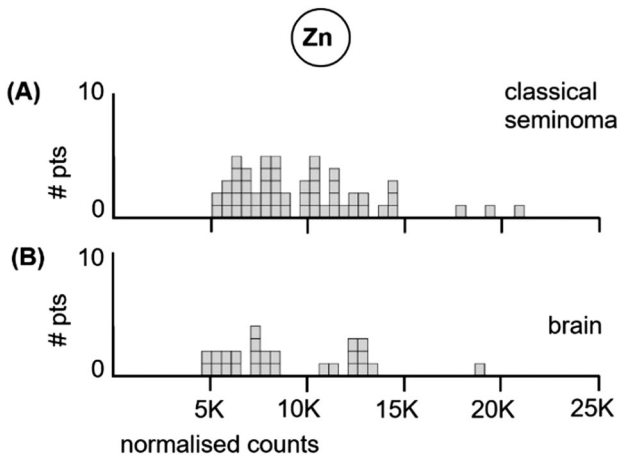

Fig. 4 Median Zn levels in tumour sections from (A) each of the 53 classical seminoma patients, and (B) each of the 26 glioblastoma patients.

We conclude from the above data that (i), classical testicular seminoma, a known clinically-inferred very radiosensitive tumour type with very high patient survival after radiation treatment, has very low median Mn levels. In contrast, (ii), glioblastoma, which represents the deadliest of all brain tumour types, and is a known clinically-inferred very radioresistant tumour type with very low patient survival, has high median Mn levels. In addition, (iii), median Zn levels neither track radioresponsiveness nor patient survival in these two tumour types. The LA-ICP-MS data are consistent with an involvement of Mn in radioresponsiveness.

2. Mn and clinically-inferred radioresistance in atypical seminomas. Although most seminomas are radiosensitive, between 5–15% consist of pathologically distinct subtypes (atypical/anaplastic) which have some degree of radioresistance. Of the 59 testicular seminomas examined herein, 53 were classical seminomas described above, while 6 were pathologically atypical, described below.

The LA-ICP-MS data of the 6 atypicals (red boxes) are shown in Fig. 5(A, B, C and D), for their Mn, Cu, Zn and Fe levels respectively. It is striking that all six atypicals had elevated Mn tumour levels (Fig. 5(B), red boxes) which did not overlap with the Mn tumour levels of the 53 classical seminomas (Fig. 5(A), green boxes). Two of these atypicals had median Mn tumour levels that exceeded 10 000 ncps. By contrast, these same six atypicals had Cu, Zn and Fe tumour levels that fell within the range of the classical seminomas for those metals, (Fig. 5(B, C and D) respectively). The atypicals are thus distinguished by their higher Mn tumour levels, while their Cu, Zn and Fe levels, with one exception, remain within the boundaries of the classical seminoma levels for each metal.

Survival data are unavailable for these 6 patients. However, examination of published data of unrelated patients with atypical seminomas who did receive radiation treatment, reveal that they have a reduced survival rate of 50–70% at 10 years.[25,28] Atypical seminomas thus have a degree of clinically-inferred radioresistance with some variation between studies.

We conclude from the above data that within the single cancer category of testicular seminoma, (i), the clinically-inferred radiosensitive classical seminomas have high patient survival and low Mn tumour levels, while the clinically-inferred radioresistant atypical seminomas have far lower patient survival and higher Mn levels. In contrast, (ii), median Cu, Zn and Fe tumour levels neither track radioresponsiveness nor patient survival in these two categories within the same tumour type. It is important to note that (iii), the primacy of Mn levels as regards clinically-inferred radioresponsiveness and patient survival, has a strong parallel in the *in vitro* data on the irradiation of purified proteins in solution: certain Mn^{2+} complexes are radioprotective for ROS damage, but Cu, Zn and Fe are not.[13] The LA-ICP-MS data are consistent with an involvement of Mn in radioresponsiveness.

3. Mn and clinically-inferred-radioresistance in melanomas. Melanomas are a pathologically and clinically heterogeneous group. This extends across all treatments, be they radiotherapy,

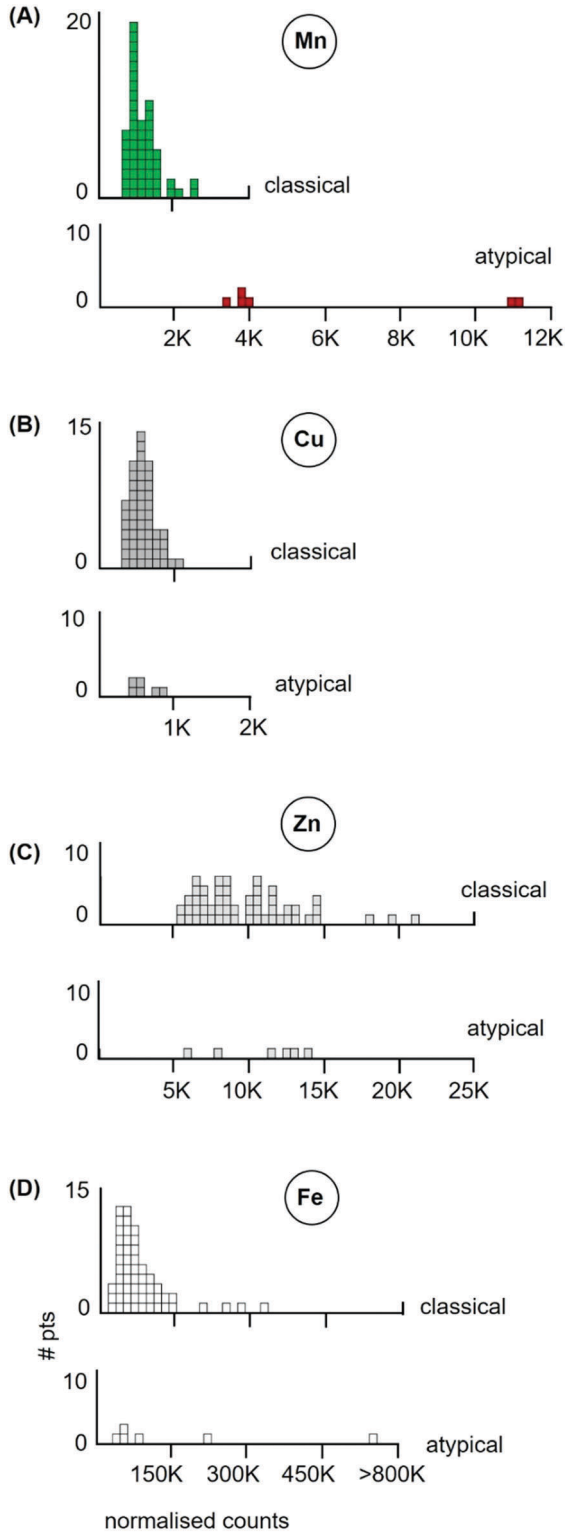

Fig. 5 Comparisons of the median Mn, Cu, Zn and Fe tumour levels from 53 patients with classical testicular seminomas (green) and six patients with atypical/anaplastic seminomas (red). The characteristics of the six atypical patients are: patient #3, (T1N0M0); patent #5, (T1N0M0); patient #34, (T4N0M0); patient #52, (T1N0M0); patient #62, (T3N0M0) and patient #69, (T1N0M0). The TNM staging system is the standard usage: T denotes the size and extent of the main tumour, N the number of lymph nodes containing abnormal cells and M the extent of metastasis to distant tissues or organs.

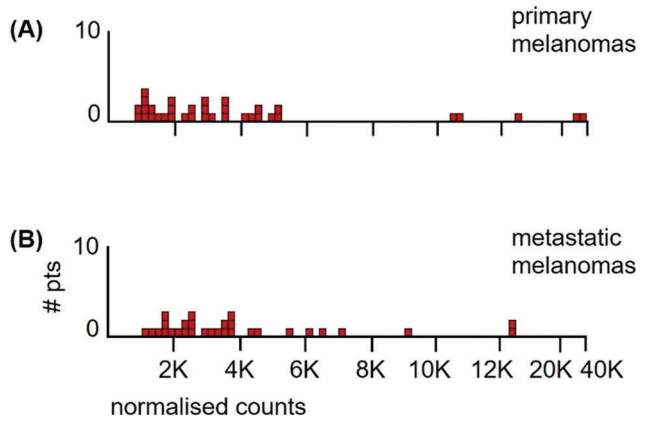

Fig. 6 Histograms of median Mn tumour levels; (A) from different primary anatomical sites of melanoma patients #81 through #120, and (B) from metastatic sites, (nearly all in lymph nodes), of melanoma patients #121 through #158.

chemotherapy, immunotherapy, or drugs. They are clinically accepted as being in the radioresistant category since radiation treatment of melanoma patients is often disappointingly inefficacious, even though some patients respond well to it.[36–38]

To determine where melanomas lie on the metallomic and the radiotherapeutic spectra, we examined tumours of 65 melanoma patients for their Mn, Cu, Zn and Fe tumour levels.

The metallomic data of the patient samples consisted of 35 primary tumours and 30 metastases from different patients. The distribution of Mn tumour levels at primary sites was not significantly different from that in metastases (Fig. 6) (Kolmogorov/Smirnov test, $D = 0.19$, $P = 0.56$). This allowed the data to be pooled.

The median Mn tumour levels of all 65 patients are shown in Fig. 7 and they are compared to those of the classical seminoma patients. The median Mn tumour level in melanomas was 2990 ncps per tumour (StDev 6020) and 31% of patients had Mn tumour levels below 2000 ncps. The two distributions differed significantly (Kolmogorov/Smirnov test, $D = 0.72$, $P = 0.00$).

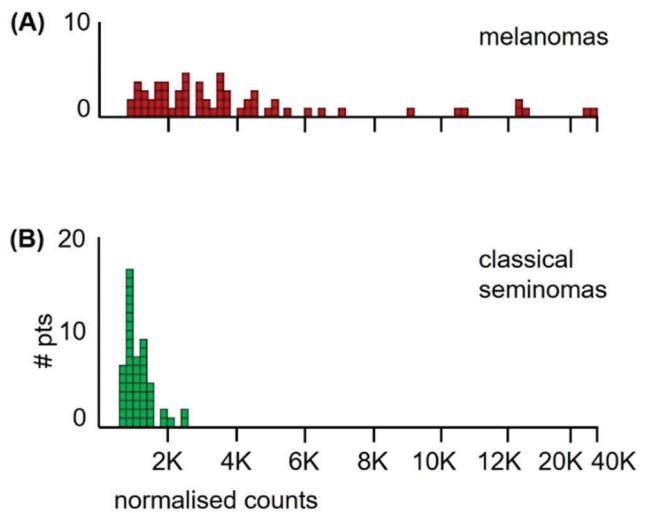

Fig. 7 Histograms of median Mn levels in tumours of; (A) all 65 melanoma patients, and (B) the 53 classical seminoma patients.

Melanomas have a large between-patient variation in Mn tumour levels with a standard deviation of 6020 compared to standard deviations of 410 for classical seminomas and 3760 for glioblastomas.

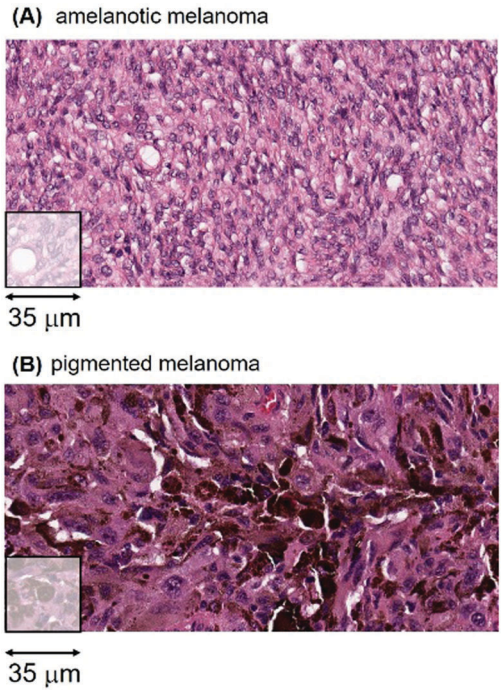

Fig. 8 Tissue sections of amelanotic and pigmented melanomas. (A) An amelanotic tumour from the forefinger of patient #109, a 54 year-old male. (B) A melanised melanoma from a lymph node of the neck of patient #122, a 29 year-old female.

There are important metallomic and clinical findings within the heterogeneity of melanomas, a major distinguishing feature being the melanin content of a tumour. Using both visual H&E staining and algorithmic criteria of melanin content, we sorted the 65 melanomas into two groups; 18 tumours with no visible or very low melanin content (herein designated amelanotic melanomas) and 47 melanomas with variable to large amounts of melanin (herein designated pigmented melanomas). Two representative examples of an amelanotic and a pigmented tumour are shown in Fig. 8.

The LA-ICP-MS Mn patient data from the 18 amelanotic and 47 pigmented melanomas are shown in Fig. 9.

The median Mn level of amelanotic tumours was 1560 ncps (StDev 799), while pigmented tumours had a median Mn tumour level of 3550 ncps (StDev 6740). Furthermore, 67% of the amelanotic tumours had Mn levels below 2000 ncps, (Fig. 9(A), light orange boxes), while only 15% of the variably pigmented tumours had Mn levels below 2000 ncps (Fig. 9(B), red boxes). Individual areas in some pigmented tumours exceeded 50 000 ncps. The two distributions differed significantly (Kolmogorov/Smirnov test, $D = 0.45$; $P = 0.004$).

Survival data were unavailable for the patients with amelanotic and pigmented tumours examined herein. However, examination of published data from unrelated patients who received radiation treatment for their metastatic tumours provided insights on overall survival.[39] Melanoma patients with amelanotic metastatic tumours had a median overall survival of ~24 months after radiotherapy, (Fig. 9(C)), compared to ~13 months for patients with pigmented metastatic tumours (Fig. 9(D)). Patients with pigmented tumours had shorter overall survival times than those whose tumours were largely devoid of melanin.

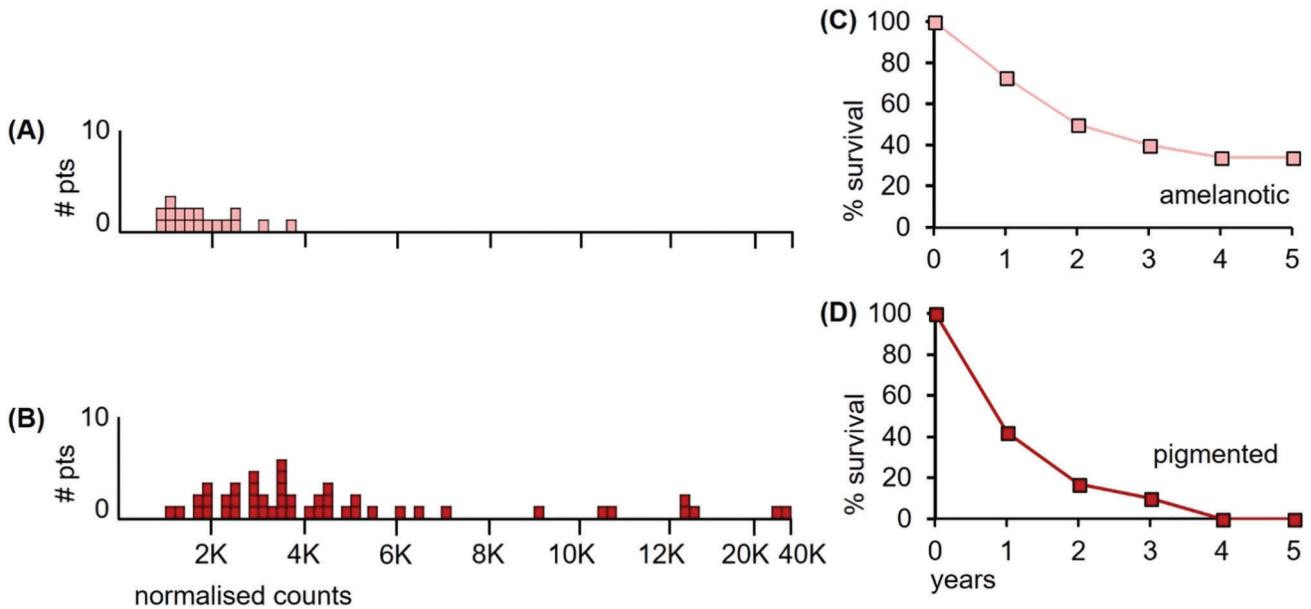

Fig. 9 Median Mn tumour levels in tissue sections of amelanotic and pigmented tumours; (A) 18 patients with amelanotic melanomas (light orange boxes); (B) 47 patients with pigmented melanomas (red boxes) with varying levels of melanin content; (C) overall survival for patients having amelanotic metastatic tumours; and (D) overall survival for patients with pigmented metastatic tumours (data for panels C and D were estimated from reference[39]).

The presence of melanin in a tumour means that interpretations of radioresistance in terms of Mn, Cu, Zn and Fe levels are not straightforward. The reason for this is that melanin chelates and stores a number of metals, including Mn (Fig. 10).

Fig. 10 reveals the concentrations of melanin in the H&E stained tissue section (Fig. 10(A)) and in the bioinformatics generated image (Fig. 10(B)). There is a clear pattern where the concentration of melanin is the highest. The four panels below show the concentrations of Mn, Cu, Zn and Fe: the highest concentrations of each metal readily superimpose on the highest melanin concentrations.

The patient survival data of Fig. 9 reveal that melanin, and/or its metallomic contents are radioprotective. However, we have not been able to deconvolute the mechanistic inputs to cellular radioresistance of pigmented melanomas since the radioprotective outcome is composed of differing contributions.

In one tumour, melanin may have chelated none or very low amounts of Mn depending on Mn availability in the bloodstream, and/or the Mn transporter levels within that tumour. In another pigmented tumour, melanin may have chelated large amounts of Mn. In addition, the contribution to radioprotection may also derive solely from Mn complexes and/or from combinations of the above.

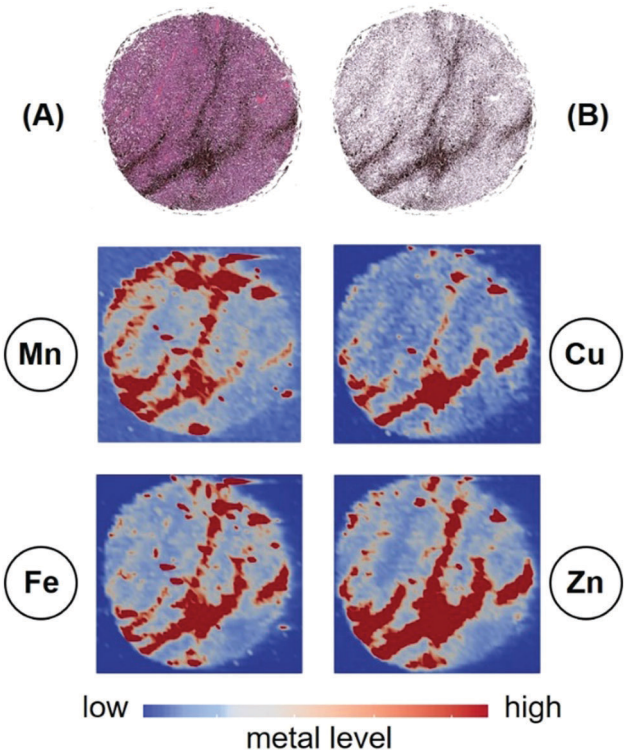

Fig. 10 H&E stained tissue section of a melanoma from the left chest wall of patient #107, (T3N0M0), with its 2D distribution of melanin, together with the 2D distribution of Mn, Cu, Fe and Zn in corresponding voxels. (A) H&E stained tissue section; (B) bioinformatics threshold analysis revealing melanin concentrations in the stained tissue section. The concentrations of Mn, Cu, Fe and Zn from identical voxels of the tumour tissue section are shown in the four panels. The colour thresholds for each of the metals in ncps are approximately; (Mn, 1000–2500 light blue/pale red, 2500–9000, red). (Cu, 200–1000 light blue/pale red, 1000–2000, red). (Zn, 4000–6000 light blue/pale red, 16 000–52 000, red). (Fe, 20 000–80 000 light blue/pale red, 80 000–200 000, red).

We conclude from the above data that (i), although melanomas have traditionally been considered as largely radioresistant in the past, they are now better appreciated as being clinically heterogeneous and spanning a wider range of radioresponsiveness. This clinical heterogeneity is reflected in the heterogeneity of the Mn data. Furthermore, (ii), irrespective of their location in the body, and irrespective of whether they are primary tumours or their metastases to lymph nodes, the melanomas exhibit a large variance in their median Mn levels. Importantly, (iii), a subset of melanomas lack detectable melanin pigment, have low Mn levels, and patients with these metastatic amelanotic tumours have higher overall survival than patients with metastatic pigmented melanomas, whose survival is relatively reduced. The LA-ICP-MS data are consistent with an involvement of Mn and/or melanin in radioresponsiveness.

4. Mn and clinically-inferred radioresistance in mesotheliomas. Mesotheliomas are a rare cancer category. We chose them for LA-ICP-MS analysis since malignant pleural mesotheliomas have traditionally been considered radiation resistant. This clinically-inferred radioresistance contrasts with the earlier work on some newly established cell lines from different patients which were radiosensitive.[40]

The current clinical situation of radiation treatment for mesothelioma patients is a controversial one. Residual gross disease cannot be eliminated even with high dose radiation, which is certainly indicative of tumour radioresistance.[41,42] However, there have been some good responses to radiation in selected patients, which is indicative of radiosensitivity.[42] Mesotheliomas thus lie in an indeterminate clinical zone wherein there is a traditional view of radioresistance, a more recent view of some radiosensitivity, and cell line data which show variable radiosensitivity. The net result is that there is no consensus on an optimal palliative radiotherapy regimen, there is variation in clinical practice worldwide, and there is variation in international guidelines.

The LA-ICP-MS Mn data from 27 mesothelioma cancer patients are shown in Fig. 11(A). The median Mn level was 2160 ncps (StDev 2840) and 44% of the mesotheliomas had Mn levels below 2000 ncps. These mesotheliomas are heterogeneous for total Mn content.

Patient survival data are unavailable for the 27 mesothelioma patients examined herein. However, such data are available from independent sources and the data from those sources are congruent. Fig. 11(B) shows patient survival data from those who first received radiation, followed by surgery. This curve differs very little from a study of two decades ago where 176 patients first underwent surgery, followed by adjuvant chemotherapy and radiation.[43] If the survival curve is taken as an indicator, then mesotheliomas are heterogenous for radiation resistance, with tumours varying from radiosensitive to radioresistant. Indeed, de Perrot *et al.*,[42] conclude that "Increasing evidence has supported that mesotheliomas are sensitive to radiation therapy".

Given that mesotheliomas are variable for Mn levels, (and for their differing clinically-inferred radioresistance), the LA-ICP-MS

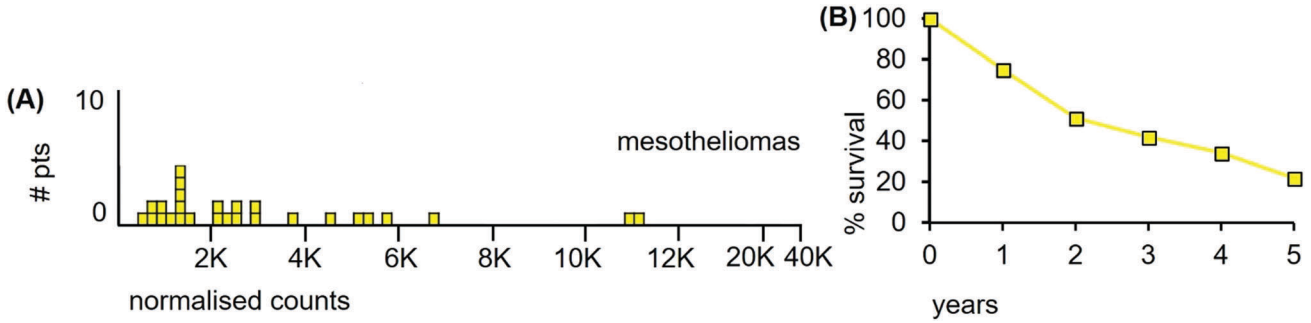

Fig. 11 (A) Median Mn levels in tissue sections from tumours of mesothelioma patients. (B) Overall survival of 90 consecutive treatment-naïve patients receiving radiotherapy followed by surgery (estimated from reference[42]).

data may be useful pointers for deciding which patient are likely to obtain the most benefit from intention-to-treat or palliative radiation treatment.

We conclude from the above data that (i), although mesotheliomas have traditionally been considered as largely radioresistant, more recent clinical evidence reveals them to be heterogeneous in terms of radioresponsiveness and patient survival. This clinical heterogeneity is reflected in Mn heterogeneity. The LA-ICP-MS data are consistent with an involvement of Mn in radioresponsiveness.

5. Mn and clinically-inferred radioresistance in small cell cancers of the lung. Small cell cancers of the lung reveal several clinical characteristics that highlight the challenges of interpreting the outcomes of radiation treatment in terms of tumour response, anatomical site and patient survival. First, cell lines of small cell lung tumours have remarkable sensitivity to even small doses of radiation, so at the tissue culture level, they are radiosensitive.[44] Second, in early (limited stage) tumours, where the cancer is still confined to the chest in a single tolerable radiation field, tumour response rates can be as high as 60–80%, so early stage tumours are definitely radiosensitive in a clinical context.[45]

The LA-ICP-MS Mn data from 21 small cell lung samples are shown in Fig. 12(A). The median Mn level was 1230 ncps (StDev 620) and 86% of the tumours had Mn levels below 2000 ncps.

Patient survival data are unavailable for the 21 patients examined herein. Since the clinical data are indicative of radiosensitivity, patient survival is expected to be high after radiation treatment. This is not the case: survival is relatively low (Fig. 12(B)). The reasons for this apparent inconsistency illustrate the variables involved in understanding tumour trajectories in multi-organ systems that impinge on patient survival.

First, the patients constituting the survival curve of Fig. 12(B) were elderly, >70 years of age, and this may be a contributing factor. Second, cancers of the lung are usually diagnosed late, because the lung is a soft and compressible organ in a fairly large cavity and there is adequate space for tumour growth without impinging on vital functions or giving rise to warning symptoms. Late detection means that cancer cells have already spread to other sites such as bone, brain or bone marrow and these metastatic lesions are usually well advanced, leading to early death. The early dissemination of small cell lung cells may be influenced by their short doubling time and high mitotic index.

We conclude from the above data that small cell lung tumours are initially radiosensitive and are low in Mn. However, their subsequent aggressive cell division properties and rapid metastatic spread throughout the lung, decouple this initial radiosensitivity from expected patient survival after radiation treatment. The LA-ICP-MS data are consistent with an involvement of Mn in radioresponsiveness.

6. Mn and clinically-inferred radioresistance in early stage prostate and breast cancers. Prostate and breast cancers have several commonalities including being two of the major secretory organs of the body. The most striking is that in both cancer types the majority of patients have high overall survival when tumours are detected early, while a minority of patients have aggressive

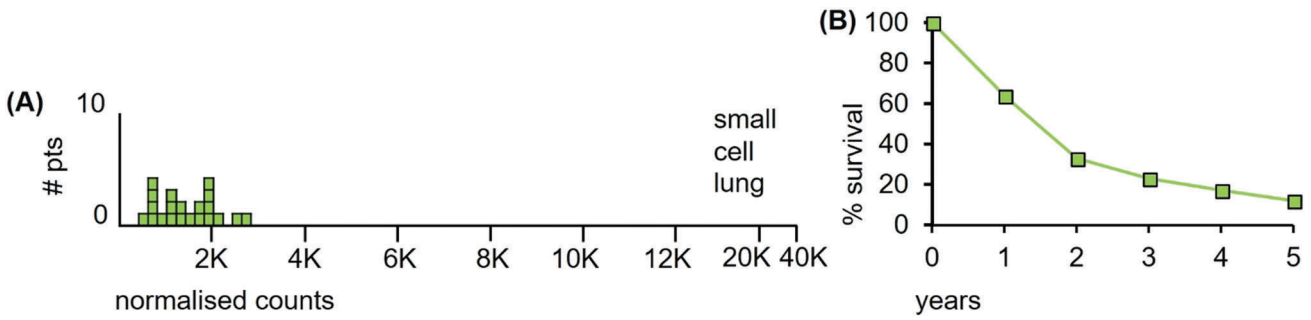

Fig. 12 (A) Median Mn levels in tissue sections from tumours of patients with small cell lung cancers. (B) Overall survival of small cell lung cancer patients (estimated from reference[46]).

cancers that respond poorly to any treatment modality and result in a low survival rate.[47]

Prostate cancer data. The LA-ICP-MS Mn data of the 16 prostate and 26 breast cancer patient samples are shown in Fig. 13(A and B) together with the 5 year survival data in panels (C and D).

Of the prostate cancer patients, 56% have tumours with median Mn level <2000 ncps. Patient survival data are unavailable for the 16 patients examined herein, but the results of the latest ProtecT clinical trial reveal that 99% of early stage prostate cancer patients who received radiotherapy as a single treatment were alive at 5 years.[48] Prostate cancer-specific mortality at 5 years is thus extremely low at $\sim$1%, (Fig. 13(C)). Previous clinical trials in this area that claimed much higher mortality rates have been shown to be compromised at multiple levels.[50,51]

The single outlier prostate cancer patient shown in Fig. 13(A) is informative in terms of his Gleason scores and grades relative to Mn levels in the remaining 15 patients. This cancer patient (#269) has a median Mn tumour level of 14 020 ncps and a Gleason score of 8. By contrast, prostate cancer patient #259 has a Mn tumour level of only 890 ncps, a 15-fold difference, yet he too has a Gleason score of 8 with the same tumour grade T4N1M1c. This finding is consistent with the data from our other tumour types, namely that Mn levels do not track tumour grade to any appreciable extent.

Breast cancer data. Of the breast cancer patients, none of whom had distant metastases, 57% had median Mn tumour levels below 2000 ncps and we infer significant radiation sensitivity. Patient survival data are unavailable for the 26 patients examined herein. However, the latest data from the National Cancer Database NCDB, (a joint project of the American College of Surgeons and the American Cancer Society), reveal that the 5 year overall survival was $\sim$93% for those patients with high risk early stage breast cancer who underwent whole breast radiotherapy after breast conserving and adjuvant chemotherapy (Fig. 13(D)).[49] The benefits of irradiating the whole breast are not in dispute, as reoccurrence of the tumour is reduced by $\sim$50% and the death rate by $\sim$16%.[52,53]

The single outlier breast cancer patient in Fig. 13(C) was informative in terms of her tumour grade relative to Mn levels in the other 20 patients. This cancer patient (#301) had a median Mn level of 11 620 ncps and a tumour grade of T2N1M0. By contrast, patient #293, had a Mn level of 1540 ncps, an $\sim$8-fold difference in Mn level, yet with a similar grade of T2N0M0. This outlier is pathologically unremarkable compared to the remaining breast cancer patients, and again, Mn levels do not track tumour grade. It is likely that the underlying generator of response to radiation is not predominantly within the traditional histopathology and immunohistochemistry areas. In this context, as revealed by the Swedish Breast Cancer Group 91 randomised clinical trial,[54] the literature on breast cancer subtypes is discordant on the effects of radiation treatment.

We conclude from the above data that (i), localized cancers of the prostate and early stage cancers of the breast, both with high patient survival after radiation treatment, have relatively low Mn levels. In addition, (ii), it is also clear that the underlying Mn-based properties of these two tumour types may be clinically more informative as regards radiation treatment than some currently utilised pathological parameters.

7. **Mn heterogeneity within tumours.** We have examined the heterogeneity within tissue sections of all seven tumour types, since we hypothesise that regions of high Mn content in

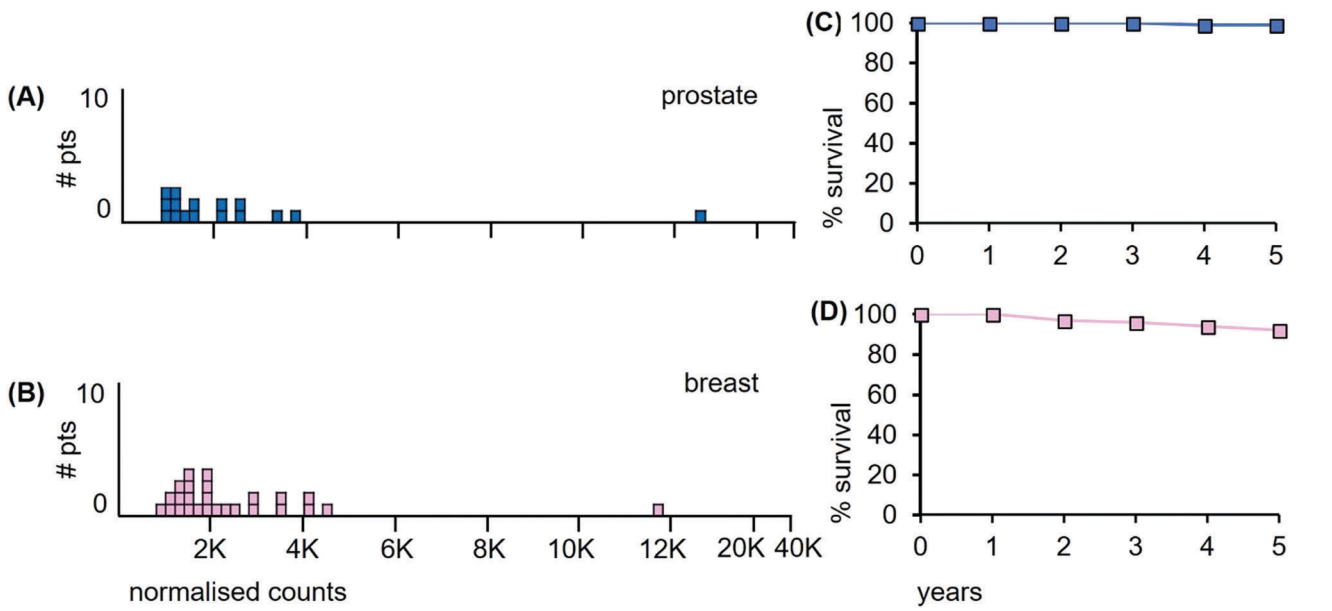

Fig. 13 Median Mn tumour levels in tissue sections from prostate and breast cancer patients. (A) 16 prostate cancer patients (pale blue); (B) 26 breast cancer patients. (C) Overall survival curve for prostate cancer patients over a 5 year period (estimated from reference[48]); (D) overall survival curve for breast cancer patients (estimated from reference[49]).

a tumour will survive radiotherapy and the tumour will likely progress, leading to reoccurrence after radiation treatment.

Heterogeneity in breast cancers. We illustrate this variation with patient #324, a 48 year-old female with invasive ductal carcinoma (Fig. 14(A)). This example highlights a number of challenges that cannot be avoided in interpreting patient data at any level, be they 'omic or non-enzymatic.

The various cell types in this tissue section are highlighted in the contrast-enhanced image of Fig. 14(B) and the H&E stained high-power microscopic image (Fig. 14(C)).

Five lymphatic vessels, c1 through c5, have been invaded by cancer cells. While the invasive cells in c1 through c4 all have median Mn levels less than 3000 ncps, the cancer cells in c5 have 8600 ncps. The invasive cells in all five lymphatic vessels appear morphologically similar, yet only the c5 group has high Mn and is potentially a radioresistant metastatic cell lineage. The immune cell region has a median Mn level of 2720 ncps, the normal breast region has a median of 3160 ncps and the adipocyte population has a median near 1000 ncps. The entire tissue sample has a median Mn level of 1740 ncps. Clearly, "grinding up/homogenizing" such a heterogeneous tumour sample for metallomic or 'omic analyses results in the pooling of the metallomic and molecular contents of at least eight different cell populations (not including other stromal cells) and completely obliterates the critical spatial information which is the basis for providing accurate estimates of clinically important parameters. Once 2D information is destroyed, there is no platform for deciding which parts of a tumour are likely to progress after radiation treatment, nor for determining the probability of tumour reoccurrence.

The heterogeneity seen here at the metallomic level has parallels with that found in different regions of primary ductal carcinomas analyzed for genome-wide copy number variation by comparative genomic hybridization.[55] Critically, neither the status of ER, PR and Her2, nor tumour grade in that study, correlated with genomic heterogeneity. Furthermore, single cell sequencing revealed that different parts of the same tumour had massive amplifications of particular genes, such as a 50-fold amplification of KRAS. Single chromosomal regions also had 30 different copy number variations, deletions and amplifications. Aneuploidy and segmental aneuploidy are common occurrences,[56] not only in tumours of the breast, but in virtually all solid tumours.

Heterogeneity in melanomas. The second example of intra-tumoural variation is illustrated by melanoma patient #112, a 48 year-old male with a malignant melanoma of the neck. Fig. 15 (A) illustrates the H&E stained tissue section that consists of both pigmented cells, extracellular melanin plus a pale staining cellular region in the top right quadrant that is

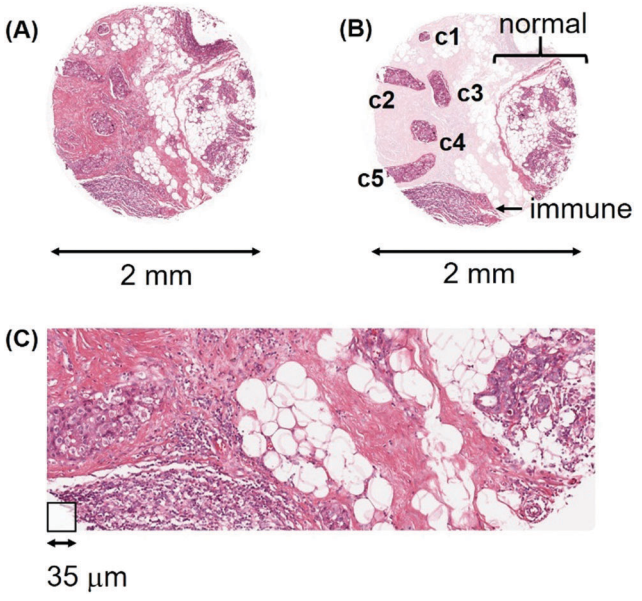

Fig. 14 (A) H&E stained section of a ductal carcinoma of the breast (T2N0M0) from patient #324 illustrating the morphological heterogeneity in a single tumour. (B) Contrast enhanced image of panel A to clearly show the various contributing cell types; (c1 through c5), 5 lymphatic vessels which have been invaded by cancer cells; adipocytes, large white spheres; normal, an area of normal ducts; immune, a concentration of invading immune cells. (C) Higher power of a track through lymphatic vessel c5, the immune cell group, adipocytes, stroma and normal ducts.

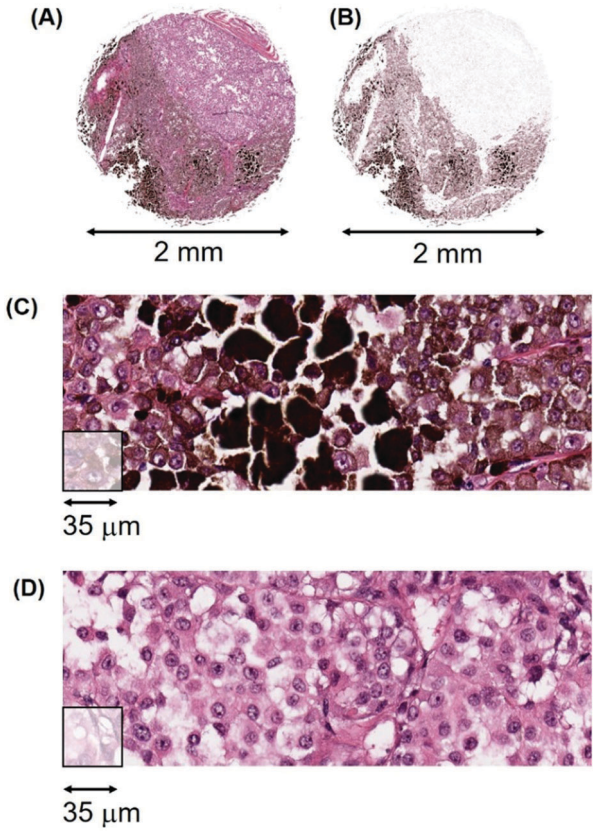

Fig. 15 (A) H&E stained section from patient #112 of a cutaneous melanoma of the neck (T2aN0M0) showing a major region of pigmentation (lower half) and a lightly staining region low in melanin (upper right quadrant); (B) 2D bioinformatics-generated image of melanin levels in individual voxels of the melanoma showing an area of low Mn, (pale) and the high and variable levels of melanin in the lower half. (C) A track through the heavily pigmented region, (D) a track through the amelanotic region.

very low in melanin (designated herein as amelanotic/low). Fig. 15(B) is a bioinformatic generated image that shows the melanin content more clearly. Fig. 15(C) illustrates high-resolution pathology tracks through the heavily pigmented region while Fig. 15(D) shows tracks through the amelanotic region.

There is a large difference in Mn content between the pigmented and amelanotic areas of this tumour, ($\sim$30 000 ncps *versus* $\sim$3000 ncps, respectively) with some pigmented areas exceeding 100 000 ncps. Approximately 50% of this tumour section has Mn values with a median of 3000 ncps.

The clinical implications of this heterogeneity for radiation treatment are as follows. If such a tumour were to be irradiated, we would expect that most of the amelanotic cells would be killed or be sufficiently damaged so as to be unable to undergo further division. The remaining radioresistant cells would repair their damage and the cancer would have a probability of $\sim$0.5 of progressing (depending on where subsequent clinical data reveal the most appropriate Mn threshold(s) to be set). The above two examples of breast and melanoma tumours reflect the importance of spatial information derived *via* LA-ICP-MS, where adequate sampling of different tissue sections will generate the 3D composition of a tumour. Since a tumour will usually also contain infiltrating immune cells, areas of blood, necrosis, fibrosis and cells undergoing apoptosis, it is necessary to take into consideration the proportion of cancer cells, and their Mn contents, in relation to each of these various populations to determine the probability of tumour reoccurrence after radiation treatment.

As illustrated by the above examples, tumours are rarely homogeneous. Cancer cells and stromal cells in a tumour are interacting dependent systems, as shown in prostate cancer cells that have metastasised to bone and are dependent upon osteoblasts in that niche to survive.[57] It is for this reason that while homogeneous tissue culture cell populations are useful for research purposes, they rarely provide prognostic clinical information of relevance to a specific patient. The lack of supporting stromal cells in tissue culture and the supply of nutrients and metals is quite unlike the supply from the harsh local environment of a tumour with its acidic and anoxic areas and the dysregulated access of metals and nutrients from a compromised vasculature.

We conclude from the above data that (i), within-tumour heterogeneity of Mn levels is one of the most critical issues that needs to be considered in the appropriate planning of radiotherapy. Furthermore, given the variation in amount and distribution of the stromal and cancerous components of a tumour, it is apparent that (ii), homogenising tumour samples to generate predictive biomarkers, will destroy, (or certainly compromise), the spatial information which is of utmost clinical importance. In this context, regions of high Mn content that are likely to survive radiation treatment, are a critical component of the information required to make prudent decisions on radiation dosages and the probability of tumour reoccurrence.

Discussion

The LA-ICP-MS data on the seven different types of cancers together with the published data on clinically-inferred radioresistance, patient survival and the published non-enzymatic catalytic chemistry of Mn interactions, are all consistent with a Mn-complexes/ROS scavenging/tumour radioresistance hypothesis.

The Mn-based data from these 7 cancer types highlight the major outcome of this study: measurements of Mn levels and their distribution in these tumour types may provide a clinically useful quantitative readout of the probability of radioresponsiveness of a particular tumour and the probability of its reoccurrence in that patient. The implications of these data may be more general. If LA-ICP-MS analyses of other tumour types also support these conclusions, then Mn-based diagnostics may turn out to be a useful pan-oncological metabolic marker in clinical radiotherapy.

It is clear that some clinicians and researchers firmly believe that the radioresistance of tumours is a property of up-regulated enzymatic DNA repair systems, up-regulated enzymatic networks involving ROS scavenging by superoxide dismutases, catalases and peroxidases, and/or mutations in genes that lead to altered proteins that confer radioresistance in tumours.

In this Discussion, we examine the relevant data bearing on these beliefs and contrast the evidence with Mn-based non-enzymatic metabolic systems that are held to underpin the data from the 7 cancer types examined herein.

DNA repair and radioresistance?

As regards the proposed primacy of enhanced enzymatic DNA repair after radiation treatment, there is a straightforward and testable prediction. Do cells up-regulate genes involved in repairing double-strand breaks, pyrimidine dimers, single-strand breaks, base damage and DNA crosslinks after radiation treatment?

Some answers are available from both tissue culture systems and patient samples. Large scale gene expression analyses on microarrays from the National Cancer Institute's set of 60 cancer cell lines, (which are derivatives of lung, melanoma, prostate, breast, colon, ovary, kidney and leukemic cells) were performed on these cell lines after ionizing radiation. Only 18 genes exhibited significantly increased expression that distinguished cell lines with a degree of radioresistance, from other cell lines, but these upregulated genes were not enriched for DNA repair genes.[58]

Gene expression analyses on irradiated breast, prostate and gliosarcoma cells also revealed that upregulated genes were not enriched for DNA repair. *Furthermore, genes upregulated in tissue culture were a different group from those that were upregulated when the same prostate cancer cell line was grown as a solid tumour and irradiated in athymic nude mice.*[59] *In vivo* up regulation also did not enrich for DNA repair.

There are now more than 177 human genes known to be involved in DNA repair,[60] however, only a handful of these are upregulated in tumours following radiation treatment.[61,62] In addition, only fragmentary reports exist on systematically connecting any upregulation of repair genes to clinically-inferred radioresistance across a diverse suite of cancer types at the same time (such as those investigated herein). Studies have generally been restricted to the in-depth examination of DNA variants in single genes such as BRCA2, in specific cancer types. What has yet to be demonstrated is the spatial transcriptomics of repair genes in tissue sections across a diverse range of clinical samples.

In irradiated yeast cultures, ''few if any of the genes involved in repairing DNA lesions produced in this study, including double-strand breaks, pyrimidine dimers, single-strand breaks, base damage and DNA crosslinks are induced in response to toxic doses of the agents that produce these lesions''.[63]

It needs to be emphasised that upregulation of a single gene rarely alters phenotype, biochemical or otherwise. It takes a coordinated network of repair enzymes to carry out DNA repair and increasing the level of a single network component is rarely productive if other members of the network remain at normal levels. The reason is that it is the flux through the network that is critical, and an upregulated single component usually leaves the output largely unchanged. Except for a dozen or so genes that render patients extremely radiosensitive when they are mutated in the germ line, the genome-centric upregulated input for tumour radioresistance remains weak.

In *in vitro* settings and bacterial studies, the consequences of radiation treatment leave little room for ambiguity. Large experimental data sets all lead to the same outcome: it is the efficient protection of the proteome from ROS, not protection of DNA, that underpins radioresistance. It is undamaged proteins that play the major role in radioresistance.[12,14–17,64] Protecting these proteins, including those involved in DNA repair, is largely *via* non-enzymatic Mn-complexes, *via* the antioxidant properties of the so called high symmetry ($H\text{-}Mn^{2+}$) complexes.[19]

We conclude that we cannot formally eliminate the possibility that the upregulation of human genes involved in DNA repair is the dominant variable that accounts for the very different radioresistance and patient survival data of the seven tumour types. However, until the 2D spatial transcriptomic data of human DNA repair genes on tissue samples become available, (using technologies such as tissue sections positioned on arrayed reverse transcription primers[65]), the clinical value of upregulated DNA repair systems remains moot.

Enzyme-based radioresistance?

An additional contribution to radioresistance could arise from the increased activity of superoxide dismutases (CuZnSOD and MnSOD), catalases and peroxidases. In this context, it needs to be noted that ~90% of the enzymatic superoxide dismutase activity normally stems from CuZnSOD, with MnSOD making a contribution of only ~10%. MnSOD is restricted to mitochondria and cannot scavenge ROS in the nucleus, while CuZnSOD is active in both the cytoplasm and the nucleus and is not so restricted.

Whole organismal data revealed that when human CuZnSOD and human catalase were upregulated in transgenic mice and those mice given 10 Gy whole body radiation, there were no significant survival differences between mice that upregulated both CuZnSOD and catalase relative to controls.[66]

When the enzymatic activities of Cu/ZnSOD and MnSOD were compared using classical enzymological assays in homogenized cancer samples in a wide range of tumours, no correlation emerged between these enzymatic activities and clinically-inferred radioresistance.[67] Second, examination of human mesothelioma biopsies for MnSOD by immunostaining of patient samples revealed no significant association between MnSOD levels and patient survival.[68] Third, assays for CuZnSOD, MnSOD, catalase and glutathione peroxidase in 31 different human cancer cell lines revealed that none of their activities were associated with resistance towards ionizing radiation.[69,70] Other examples from the large literature on superoxide dismutases, mainly in genetically engineered cell lines, demonstrate that increasing MnSOD gene dosage does lead to increased radioresistance in experimentally manipulated systems.[71,72] In human tissue samples, there can be a decrease in both CuZnSOD and MnSOD, an increase in MnSOD, no difference in CuZnSOD, or decreases in catalase.[73–75] Crucially, what is yet to be demonstrated is the 2D spatial enzymology of CuZnSOD, MnSOD, catalases and peroxidases in tissue sections across a diverse range of clinical samples.

We conclude that we cannot formally eliminate the possibility that the upregulation of these enzymatic scavengers of ROS is the dominant variable that accounts for the very different radioresistance and patient survival data of the seven tumour types. Once again, until the spatial enzymology on human tissue samples becomes available, the clinical significance of the upregulation of enzymatic scavengers of ROS, while unlikely, cannot be discounted.

Non-enzymatic ROS scavengers and radioresistance?

The LA-ICP-MS data revealed that Mn was the distinguishing metal in its association with clinically-inferred radioresistance and patient survival, while Cu, Zn and Fe revealed no consistent associations. This primacy of Mn was a consistent finding. One can ask therefore whether the clinically-inferred radioprotective effects of high Mn levels in our LA-ICP-MS data have a parallel in systems that allow the fundamental principles of metallomic interactions to be evaluated under conditions where input variables are strictly controlled. One such platform is *in vitro* radiochemistry: the irradiation of purified proteins in defined buffers together with combinations of small molecules and metals. This allows precise measurements of the efficacy of different antioxidant complexes against damaging ROS.

Some of these parallels to the LA-ICP-MS data, although distant, are striking in their revelation of fundamentally conserved principles. When glutamine synthetase (GS) was irradiated in phosphate buffer alone it suffered considerable damage from ROS, with recoverable enzymatic activity being 50% at 100 Gy.[13] The addition of Mn^{2+} and a nucleoside protected against protein damage: 50% enzymatic activity was now retained at 10 000 Gy. In this particular case, it was the spontaneous formation of the triple complex, Mn^{2+}-uridine-orthophosphate, that was the key radioprotectant. Under these same conditions, there were no protective effects of note with Cu^{2+}, Zn^{2+} or Fe^{2+}.[13]

Antioxidant activities have also been measured in a different *in vitro* chemical system, namely that of metal-drug complexes. For example, mefenamic acid is a nonsteroidal anti-inflammatory drug which acts as a free radical scavenger and its properties are enhanced when it is complexed with various metals. It is the mefenamic acid complex with Mn that has the highest scavenging activity, exceeding that of the Cu- and Zn-mefenamic complexes.[76]

Radioprotective supremacy: Mn-peptide complexes

The most potent antioxidant Mn^{2+}-complexes found to date are those in combination with peptides.[13] Thus, a particular decapeptide in potassium phosphate or sodium bicarbonate buffer with Mn^{2+}, protects glutamine synthetase activity even more strongly than Mn^{2+}-complexes with nucleosides, with 50% activity retained at $\sim$50 000 Gy. Decapeptides are readily taken up by cells in tissue culture and in mice, and one such tripartite Mn^{2+}-peptide-orthophosphate complex is the most effective radioprotectant so far known. Not only is the survival of irradiated cells in culture massively increased, but so also is the survival of mice given whole body radiation.[18]

The existence of radioprotective Mn^{2+}-complexes with peptides has significant implications for tumour radiotherapeutics. Tumours have anoxic/hypoxic regions and areas of cell death where there is no shortage of dying cells and their autoproteolytic digests. This is evident in the large necrotic areas of many tumours, such as glioblastomas (for example, in Fig. 3). In such an environment of cell death and of variation-selection processes, the surviving cells have access to an increased supply of metabolites including peptides, phosphates, nucleosides, free amino acids and all manner of metabolites. Thus, it only requires uptake of Mn from the bloodstream to automatically produce non-enzymatic, ROS-scavenging, complexes. The equilibrium of complex formation is greatly in their favour, with metabolites in the millimolar range and Mn in the micromolar range.

Depending on the level of Mn in the bloodstream and the levels of Mn transporters in tumour cells, some tumours will unavoidably accumulate more Mn than others. Different cells within a tumour, as well as tumours in different individuals, will have different concentrations of Mn^{2+}-complexes with different metabolites.

The results of this natural sequence of molecular events are seen in the context of Mn uptake in normal tissues and organs and their cancerous derivatives.

Mn uptake and its distribution in normal tissues/organs

Under normal conditions, nearly all Mn enters the human body from the gastrointestinal tract *via* the hepatic portal vein and is taken up by the liver, while excess Mn is exported *via* the bile duct into the small intestine. This dual system controls Mn levels in the blood *via* the influx and efflux metal transporters in the liver and bile duct epithelium: predominantly *via* SLC39A14 (Mn uptake by the liver) and SLC30A10 (Mn efflux *via* the bile duct epithelium).[23,24] If these transporters are altered by mutation, allelic variants, or regulatory elements, the level of Mn in the blood is changed. When this occurs, dietary Mn uptake by the liver is reduced, more Mn is directed into the blood, and higher than normal concentrations accumulate in organs such as the brain.

We found that Mn levels were highest in normal liver and pancreas but lower in cardiac muscle, cerebral cortex and spleen (ESI,† Table S3). These levels agree with other methods, reinforcing the finding that Mn content in tissue sections measured *via* LA-ICP-MS is a reflection of *in vivo* content, and not an artefact of fixation or metal loss. Importantly, ESI,† Table S3 illustrates the Mn content in organs of three healthy individuals, #341, #342 and #333 where two different anatomical regions have been sampled from the same individual and hence are in the same genetic background. These data provide an initial insight into LA-ICP-MS determined Mn levels between different normal tissues and organs in healthy individuals.

Mn uptake and its distribution in tumours

The quantities of Mn that are released into the bloodstream are directly consequential to the uptake of Mn by tumours, irrespective of whether the tumours are primary or distant metastases (as revealed in Fig. 6 with primary and metastatic melanomas). Mn levels will depend on blood supply to the tumour, access to, and leakiness of the tumour vasculature, and the expression levels of the influx/efflux transporters in cells in different parts of the tumour.

While the normal liver and normal bile duct Mn transporters are products of normal genomic balance, nearly all solid tumours have grossly reorganised genomes carrying amplifications, deletions, inversions, translocations and epigenetic modifications. They are aneuploid and segmentally aneuploid. This has significant ramifications for radioresistance of tumours. For example, the determinant of how much Mn is available to cells within a tumour, (both cancerous and stromal cells) is first dependent upon how much Mn has been released into the bloodstream. This will depend on the allelic variants in the transporters of that specific individual and the dietary intake of Mn for that individual.

The level of Mn in a tumour thus depends on the extent to which the transporter genes are amplified, deleted or dysregulated, resulting in over- or under-expression of their transporter proteins. Owing to the truly massive genomic reorganization in most tumour cells, it is unavoidable that influx and efflux transporters will vary in copy number (from being homozygously deleted to multiple copies; 0, 1, 2, 3, 4, *etc.*) in different tumour cells. This will result in different Mn influxes and effluxes in different cells in a tumour.

In summary, each individual will have a certain amount of Mn entering the bloodstream which is available for tumour uptake. Depending on the expression level of influx and efflux transporters in that tumour, at that time, a particular level of Mn is reached as a result of natural biochemical processes. It is merely extraction efficiency from the blood, and retention within tumours, that are the underlying forces.

We conclude that this non-enzymatic antioxidant system based on Mn^{2+}-complexes arises naturally, and proceeds inexorably, as a result of the liver/biliary gateway and the dietary supply of Mn^{2+}. It leads to variation in the levels of Mn^{2+}-complexes in different tumours and provides a pre-loaded system for ameliorating damage from ROS. When a tumour is irradiated, this frontline cellular defence and cleaning system is instantaneously available for protection of the proteome unlike the time delay for the induction and upregulation of genes for DNA repair and enzymatic ROS scavenging genes.

Conclusions and future implications

Given the above data from LA-ICP-MS, from DNA repair, from enzymological scavenging and from non-enzymatic Mn-based antioxidant systems, the Mn-complexes/ROS scavenging/tumour radioresistance hypothesis is currently the most plausible. It provides an intellectual framework in radiation tumour biology of the type sought by Gatenby[4] and is testable *via* randomised clinical trials or initially by sequential testing of patients of any tumour type for whom radiation treatment is the appropriate option.

To facilitate a practical clinical connection, we outline an LA-ICP-MS strategy using the metallomic and molecular cartography of tumours that may be helpful. This is placed into context with current radiation regimens that largely treat cancer patients within a single tumour type as a near uniform homogeneous cohort.

The final goals: beyond the one-size-fits-all approach to patient treatment

The current situation in radiation treatment of a patient is exemplified by adjuvant radiotherapy for breast cancer in the UK and the USA. In the UK a standardised protocol of 50 Gy is delivered in 25 fractions of 2 Gy each over a period of 5 weeks while in the USA it similar: 40 Gy in 15 fractions, or 42.5 Gy in 16 fractions.[77,78] Standardised protocols are the norm for other cancers, with each tumour category having its own specific dosages and fractions. The issue with such generic treatment, as the LA-ICP-MS 2D spatial data have revealed, is that it does not deal with the considerable heterogeneity within each tumour type.

If tumour radioresistance turns out to be predominantly determined by Mn and the sizes of pools of metabolites, then the first task is to generate a quantitative readout of the probability of radioresistance of any tumour so that a physician can tailor a suitable treatment that goes beyond the one-size-fits-all approach (Fig. 16). Given that a single ablation track across a 1 mm tumour section can be completed in ~7 seconds, regions of interest on a standard pathology slide can be analysed in minutes to obtain an overview of tumour heterogeneity *via* metallomic inhomogeneities. The second task is to determine the threshold(s), below and above which the radiation dose can be so adjusted so as to provide maximum killing power to the tumour, and the minimum to nearby healthy tissues and organs. This can be found empirically, either *via* conventional randomised clinical trials, or by correlating patient outcomes in a single tumour type where heterogeneity is extreme.

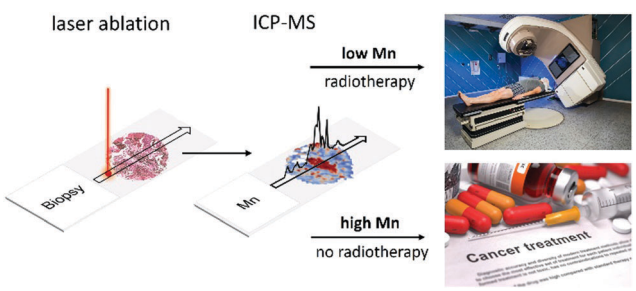

Fig. 16 Proposed diagnostic scheme. A paraffin embedded patient biopsy is analysed by LA-ICP-MS for quantification of Mn. An appropriate threshold of Mn determines a patient's suitability for radiation therapy, or a choice of other treatments.

The foundation for both these tasks lies in the use of Mn determinations and metal-labelled probes to generate a multi-layered cartography of tumour tissue sections.

Multimodal cartography

Any molecular entity, be it antibody, nucleic acid, or drug, can be tagged with different metals[79,80] and hybridised to adjacent human tissue sections so as to reveal their localised concentrations relative to the positional coordinates of Mn. The power of Mn maps is that they can be overlaid with other metal-based maps, such as that of the distribution of drug targets, antibodies and immune cells. The result is a multi-level cartographic output that integrates potential radiation information with other clinically significant modalities. These can include the distribution of the ER, PR and HER2 receptors in breast cancer, cell division markers such as Ki-67, immune system markers such as PD-1 and PD-L1 or any of the currently "actionable drivers" of tumour progression found from genomic analyses, such as mutated BRAF in melanoma.

These multi-layered maps can be integrated *via* automated image scanning technology and machine learning algorithms to provide clinically informative quantitative insights into the global properties of that particular tumour. The rapid acquisition of multiple features in routine pathological processing laboratories using LA-ICP-MS instrumentation may help radiation oncologists to better tailor the appropriate radiation dosage to individual patients to increase overall survival.

Author contributions

The laser ablation work was generated on a fee-for-service basis agreement between GLGM and the University of Technology Sydney, Australia. GLGM and PD performed data analyses and discussed technical and scientific results that were in the public domain. Both authors wrote the manuscript.

Conflicts of interest

GLGM declares the following interest. GLGM conceived and personally funded the study and retains the Intellectual Property rights, granted patents AU2016222299B1 and AU2017201731B2, and International Patent # WO 2017/004684 A1 now assigned to Atomic Oncology Pty Ltd.

Acknowledgements

We thank I. E. Haines, (AMREP Department of Medicine, Alfred hospital, Melbourne, Australia and Senior Medical Oncologist and Palliative Care Physician, Melbourne Oncology Group, Cabrini Hospital, Monash University, Melbourne, Australia) for expert clinical guidance; P. A. Baird, (senior private pathologist Sydney, Australia), for teaching aspects of H&E tissue interpretation

to GLGM; US Biomax for clarification of cancer tissue sections; E. Fischer and A. Bendich (University of Washington, Seattle, USA) for biochemical input and improvements on a preliminary version of this manuscript; A. Drukier for insights on radiation physics and J. Flattery-O'Brien (Shelston IP, Sydney Australia) for legal and scientific advice. PAD is the recipient of an Australian Research Council Discovery Project (DP170100036).

Notes and references

1 B. D. Kavanagh, B. G. Haffty and J. E. Tepper, Radiation oncology: a snapshot in time, 2014, *J. Clin. Oncol.*, 2014, **32**, 2825–2826.
2 J. G. Scott, A. Berglund, M. J. Schell, I. Mihaylov, W. J. Fulp, B. Yue, E. Welsh, J. J. Caudell, K. Ahmed, T. S. Strom, E. Mellon, P. Venkat, P. Johnstone, J. Foekens, J. Lee, E. Moros, W. S. Dalton, S. A. Eschrich, H. McLeod, L. B. Harrison and J. F. Torres-Roca, A genome-based model for adjusting radiotherapy dose (GARD): a retrospective, cohort-based study, *Lancet Oncol.*, 2017, **18**, 202–211.
3 J. Lacombe, D. Azria, A. Mange and J. Solassol, Proteomic approaches to identify biomarkers predictive of radiotherapy outcomes, *Expert Rev. Proteomics*, 2013, **10**, 33–42.
4 R. Gatenby, Perspective: finding cancer's first principles, *Nature*, 2012, **491**, S55.
5 E. M. Gregory and I. Fridovich, Oxygen Metabolism in Lactobacillus plantarum, *J. Bacteriol.*, 1974, **117**, 166–169.
6 F. S. Archibald and I. Fridovich, Manganese and Defenses against Oxygen Toxicity in Lactobacillus plantarum, *J. Bacteriol.*, 1981, **145**, 442–451.
7 F. S. Archibald and I. Fridovich, The scavenging of superoxide radical by manganous complexes: in vitro, *Arch. Biochem. Biophys.*, 1982, **214**, 452–463.
8 E. R. Stadtman, B. S. Berlett and P. B. Chock, Manganese-dependent disproportionation of hydrogen peroxide in bicarbonate buffer, *Proc. Natl. Acad. Sci. U. S. A.*, 1990, **87**, 384–388.
9 B. S. Berlett, P. B. Chock, M. B. Yim and E. R. Stadtman, Manganese(II) catalyzes the bicarbonate-dependent oxidation of amino acids by hydrogen peroxide and the amino acid-facilitated dismutation of hydrogen peroxide, *Proc. Natl. Acad. Sci. U. S. A.*, 1990, **87**, 389–393.
10 E. R. Stadtman and B. S. Berlett, Fenton chemistry. Amino acid oxidation, *J. Biol. Chem.*, 1991, **266**, 17201–17211.
11 K. Barnese, E. B. Gralla, J. S. Valentine and D. E. Cabelli, Biologically relevant mechanism for catalytic superoxide removal by simple manganese compounds, *Proc. Natl. Acad. Sci. U. S. A.*, 2012, **109**, 6892–6897.
12 M. J. Daly, E. K. Gaidamakova, V. Y. Matrosova, A. Vasilenko, M. Zhai, R. D. Leapman, B. Lai, B. Ravel, S. M. Li, K. M. Kemner and J. K. Fredrickson, Protein oxidation implicated as the primary determinant of bacterial radioresistance, *PLoS Biol.*, 2007, **5**, e92.
13 M. J. Daly, E. K. Gaidamakova, V. Y. Matrosova, J. G. Kiang, R. Fukumoto, D. Y. Lee, N. B. Wehr, G. A. Viteri, B. S. Berlett and R. L. Levine, Small-molecule antioxidant proteome-shields in Deinococcus radiodurans, *PLoS One*, 2010, **5**, e12570.
14 A. Krisko and M. Radman, Protein damage and death by radiation in Escherichia coli and Deinococcus radiodurans, *Proc. Natl. Acad. Sci. U. S. A.*, 2010, **107**, 14373–14377.
15 D. Slade and M. Radman, Oxidative stress resistance in Deinococcus radiodurans, *Microbiol. Mol. Biol. Rev.*, 2011, **75**, 133–191.
16 M. J. Daly, Death by protein damage in irradiated cells, *DNA Repair*, 2012, **11**, 12–21.
17 A. Krisko and M. Radman, Biology of extreme radiation resistance: the way of Deinococcus radiodurans, *Cold Spring Harbor Perspect. Biol.*, 2013, **5**, a012765.
18 P. Gupta, M. Gayen, J. T. Smith, E. K. Gaidamakova, V. Y. Matrosova, O. Grichenko, B. Knollmann-Ritschel, M. J. Daly, J. G. Kiang and R. K. Maheshwari, MDP: A Deinococcus Mn2+–Decapeptide Complex Protects Mice from Ionizing Radiation, *PLoS One*, 2016, **11**, e0160575.
19 A. Sharma, E. K. Gaidamakova, O. Grichenko, V. Y. Matrosova, V. Hoeke, P. Klimenkova, I. H. Conze, R. P. Volpe, R. Tkavc, C. Gostincar, N. Gunde-Cimerman, J. DiRuggiero, I. Shuryak, A. Ozarowski, B. M. Hoffman and M. J. Daly, Across the tree of life, radiation resistance is governed by antioxidant Mn(2+), gauged by paramagnetic resonance, *Proc. Natl. Acad. Sci. U. S. A.*, 2017, **114**, E9253–E9260.
20 J. Lear, D. Hare, P. Adlard, D. Finkelstein and P. Doble, Improving acquisition times of elemental bio-imaging for quadrupole-based LA-ICP-MS, *J. Anal. At. Spectrom.*, 2012, **27**, 159–164.
21 S. D. Tanner, V. I. Baranov and D. R. Bandura, Reaction cells and collision cells for ICP-MS: a tutorial review, *Spectrochim. Acta, Part B*, 2002, **57**, 1361–1452.
22 D. Hare, F. Burger, C. Austin, F. Fryer, R. Grimm, B. Reedy, R. A. Scolyer, J. F. Thompson and P. Doble, Elemental bio-imaging of melanoma in lymph node biopsies, *Analyst*, 2009, **134**, 450–453.
23 S. Jenkitkasemwong, A. Akinyode, E. Paulus, R. Weiskirchen, S. Hojyo, T. Fukada, G. Giraldo, J. Schrier, A. Garcia, C. Janus, B. Giasson and M. D. Knutson, SLC39A14 deficiency alters manganese homeostasis and excretion resulting in brain manganese accumulation and motor deficits in mice, *Proc. Natl. Acad. Sci. U. S. A.*, 2018, **115**, E1769–E1778.
24 Y. Nishito, N. Tsuji, H. Fujishiro, T. A. Takeda, T. Yamazaki, F. Teranishi, F. Okazaki, A. Matsunaga, K. Tuschl, R. Rao, S. Kono, H. Miyajima, H. Narita, S. Himeno and T. Kambe, Direct Comparison of Manganese Detoxification/Efflux Proteins and Molecular Characterization of ZnT10 Protein as a Manganese Transporter, *J. Biol. Chem.*, 2016, **291**, 14773–14787.
25 V. S. Bobba, B. B. Mittal, S. V. Hoover and A. Kepka, Classical and anaplastic seminoma: difference in survival, *Radiology*, 1988, **167**, 849–852.
26 J. Classen, H. Schmidberger, C. Meisner, R. Souchon, M. L. Sautter-Bihl, R. Sauer, S. Weinknecht, K. U. Kohrmann and M. Bamberg, Radiotherapy for stages IIA/B testicular seminoma: final report of a prospective multicenter clinical trial, *J. Clin. Oncol.*, 2003, **21**, 1101–1106.

27 G. M. Mead, S. D. Fossa, R. T. Oliver, J. K. Joffe, R. A. Huddart, J. T. Roberts, P. Pollock, R. Gabe, S. P. Stenning and M. E. S. T. Collaborators, Randomized trials in 2466 patients with stage I seminoma: patterns of relapse and follow-up, *J. Natl. Cancer Inst.*, 2011, **103**, 241–249.

28 L. Serdar, E. Canyilmaz, T. O. Topcu, A. Sahbaz, Y. Memis, G. Soydemir, O. Aynaci, M. Kandaz, Z. Bahat and A. Yoney, Adjuvant radiotherapy in stage 1 seminoma: evaluation of prognostic factors and results of survival, *J. Cancer Res. Ther.*, 2015, **11**, 313–318.

29 R. A. W. van de Wetering, S. Sleijfer, D. R. Feldman, S. A. Funt, G. J. Bosl and R. de Wit, Controversies in the Management of Clinical Stage I Seminoma: Carboplatin a Decade in-Time to Start Backing Out, *J. Clin. Oncol.*, 2018, **36**, 837–840.

30 K. Kelley, J. Knisely, M. Symons and R. Ruggieri, Radioresistance of Brain Tumors, *Cancers*, 2016, **8**, 42.

31 P. Navarria, F. Pessina, S. Tomatis, R. Soffietti, M. Grimaldi, E. Lopci, A. Chiti, A. Leonetti, A. Casarotti, M. Rossi, L. Cozzi, A. M. Ascolese, M. Simonelli, S. Marcheselli, A. Santoro, E. Clerici, L. Bello and M. Scorsetti, Are three weeks hypofractionated radiation therapy (HFRT) comparable to six weeks for newly diagnosed glioblastoma patients? Results of a phase II study, *Oncotarget*, 2017, **8**, 67696–67708.

32 M. L. Biggs and S. M. Schwartz, *Cancer survival among adults: US SEER Program, 1988–2001: patient and tumor characteristics*, National Cancer Institute (NCI), Bethesda, 2007.

33 J. S. Barnholtz-Sloan, A. E. Sloan and A. G. Schwartz, *Cancer survival among adults: US SEER Program, 1988–2001: patient and tumor characteristics*, National Cancer Institute (NCI), Bethesda, 2007.

34 M. V. Zoriy, M. Dehnhardt, G. Reifenberger, K. Zilles and J. S. Becker, Imaging of Cu, Zn, Pb and U in human brain tumor resections by laser ablation inductively coupled plasma mass spectrometry, *Int. J. Mass Spectrom.*, 2006, **257**, 27–33.

35 M. Uhlen, C. Zhang, S. Lee, E. Sjostedt, L. Fagerberg, G. Bidkhori, R. Benfeitas, M. Arif, Z. Liu, F. Edfors, K. Sanli, K. von Feilitzen, P. Oksvold, E. Lundberg, S. Hober, P. Nilsson, J. Mattsson, J. M. Schwenk, H. Brunnstrom, B. Glimelius, T. Sjoblom, P. H. Edqvist, D. Djureinovic, P. Micke, C. Lindskog, A. Mardinoglu and F. Ponten, A pathology atlas of the human cancer transcriptome, *Science*, 2017, **357**, eaan2507.

36 A. Mahadevan, V. L. Patel and N. Dagoglu, Radiation Therapy in the Management of Malignant Melanoma, *Oncology*, 2015, **29**, 743–751.

37 E. K. Rofstad, Radiation Biology of Malignant Melanoma, *Acta Radiol.: Oncol.*, 2009, **25**, 1–10.

38 M. J. Sambade, E. C. Peters, N. E. Thomas, W. K. Kaufmann, R. J. Kimple and J. M. Shields, Melanoma cells show a heterogeneous range of sensitivity to ionizing radiation and are radiosensitized by inhibition of B-RAF with PLX-4032, *Radiother. Oncol.*, 2011, **98**, 394–399.

39 A. A. Brozyna, W. Jozwicki, K. Roszkowski, J. Filipiak and A. T. Slominski, Melanin content in melanoma metastases affects the outcome of radiotherapy, *Oncotarget*, 2016, **7**, 17844–17853.

40 A.-M. Häkkinenm, A. Laasonen, K. Linnainmaa, K. Mattson and S. Pyrhonen, Radiosensitivity of Mesothelioma Cell Lines, *Acta Oncol.*, 2009, **35**, 451–456.

41 H. L. Kindler, N. Ismaila, S. G. Armato, 3rd, R. Bueno, M. Hesdorffer, T. Jahan, C. M. Jones, M. Miettinen, H. Pass, A. Rimner, V. Rusch, D. Sterman, A. Thomas and R. Hassan, Treatment of Malignant Pleural Mesothelioma: American Society of Clinical Oncology Clinical Practice Guideline, *J. Clin. Oncol.*, 2018, **36**, 1343–1373.

42 M. d. Perrot, L. Wu, M. Wu and B. C. J. Cho, Radiotherapy for the treatment of malignant pleural mesothelioma, *Lancet Oncol.*, 2017, **18**, e532–e542.

43 D. J. Sugarbaker, R. M. Flores, M. T. Jaklitsch, W. G. Richards, G. M. Strauss, J. M. Corson, M. M. DeCamp, Jr., S. J. Swanson, R. Bueno, J. M. Lukanich, E. H. Baldini and S. J. Mentzer, Resection margins, extrapleural nodal status, and cell type determine postoperative long-term survival in trimodality therapy of malignant pleural mesothelioma: results in 183 patients, *J. Thorac. Cardiovasc. Surg.*, 1999, **117**, 54–63; discussion 63–55.

44 D. N. Carney, J. B. Mitchell and T. J. Kinsella, *In vitro* radiation and chemotherapy sensitivity of established cell lines of human small cell lung cancer and its large cell morphological variants, *Cancer Res.*, 1983, **43**, 2806–2811.

45 M. C. Pietanza, L. A. Byers, J. D. Minna and C. M. Rudin, Small cell lung cancer: will recent progress lead to improved outcomes?, *Clin. Cancer Res.*, 2015, **21**, 2244–2255.

46 C. D. Corso, C. E. Rutter, H. S. Park, N. H. Lester-Coll, A. W. Kim, L. D. Wilson, Z. A. Husain, R. C. Lilenbaum, J. B. Yu and R. H. Decker, Role of Chemoradiotherapy in Elderly Patients With Limited-Stage Small-Cell Lung Cancer, *J. Clin. Oncol.*, 2015, **33**, 4240–4246.

47 L. Tabar, P. B. Dean, A. M. Yen, M. Tarjan, S. Y. Chiu, S. L. Chen, J. C. Fann and T. H. Chen, A Proposal to Unify the Classification of Breast and Prostate Cancers Based on the Anatomic Site of Cancer Origin and on Long-term Patient Outcome, *Breast Cancer*, 2014, **8**, 15–38.

48 F. C. Hamdy, J. L. Donovan, J. A. Lane, M. Mason, C. Metcalfe, P. Holding, M. Davis, T. J. Peters, E. L. Turner, R. M. Martin, J. Oxley, M. Robinson, J. Staffurth, E. Walsh, P. Bollina, J. Catto, A. Doble, A. Doherty, D. Gillatt, R. Kockelbergh, H. Kynaston, A. Paul, P. Powell, S. Prescott, D. J. Rosario, E. Rowe, D. E. Neal and T. S. G. Protec, 10-Year Outcomes after Monitoring, Surgery, or Radiotherapy for Localized Prostate Cancer, *N. Engl. J. Med.*, 2016, **375**, 1415–1424.

49 A. C. Moreno, Y. H. Lin, I. Bedrosian, Y. Shen, M. C. Stauder, B. D. Smith, T. A. Buchholz, G. V. Babiera, W. A. Woodward and S. F. Shaitelman, Use of regional nodal irradiation and its association with survival for women with high-risk, early stage breast cancer: A National Cancer Database analysis, *Adv. Radiat. Oncol.*, 2017, **2**, 291–300.

50 I. E. Haines, R. J. Ablin and G. L. Miklos, Screening for prostate cancer: time to put all the data on the table, *BMJ*, 2016, **353**, i2574.

51 I. E. Haines and G. L. Gabor Miklos, Prostate-specific antigen screening trials and prostate cancer deaths: the

androgen deprivation connection, *J. Natl. Cancer Inst.*, 2013, **105**, 1534–1539.

52 S. Darby, P. McGale, C. Correa, C. Taylor, R. Arriagada, M. Clarke, D. Cutter, C. Davies, M. Ewertz, J. Godwin, R. Gray, L. Pierce, T. Whelan, Y. Wang and R. Peto, Effect of radiotherapy after breast-conserving surgery on 10 year recurrence and 15 year breast cancer death: meta-analysis of individual patient data for 10 801 women in 17 randomised trials, *Lancet*, 2011, **378**, 1707–1716.

53 C. T. P. McGale, C. Correa, D. Cutter, F. Duane, M. Ewertz, R. Gray, G. Mannu, R. Peto, T. Whelan, Y. Wang, Z. Wang and S. Darby, Effect of radiotherapy after mastectomy and axillary surgery on 10 year recurrence and 20 year breast cancer mortality: meta-analysis of individual patient data for 8135 women in 22 randomised trials, *Lancet*, 2014, **383**, 2127–2135.

54 M. Sjostrom, D. Lundstedt, L. Hartman, E. Holmberg, F. Killander, A. Kovacs, P. Malmstrom, E. Nimeus, E. Werner Ronnerman, M. Ferno and P. Karlsson, Response to Radiotherapy After Breast-Conserving Surgery in Different Breast Cancer Subtypes in the Swedish Breast Cancer Group 91 Radiotherapy Randomized Clinical Trial, *J. Clin. Oncol.*, 2017, **35**, 3222–3229.

55 N. Navin, A. Krasnitz, L. Rodgers, K. Cook, J. Meth, J. Kendall, M. Riggs, Y. Eberling, J. Troge, V. Grubor, D. Levy, P. Lundin, S. Maner, A. Zetterberg, J. Hicks and M. Wigler, Inferring tumor progression from genomic heterogeneity, *Genome Res.*, 2010, **20**, 68–80.

56 N. Navin, J. Kendall, J. Troge, P. Andrews, L. Rodgers, J. McIndoo, K. Cook, A. Stepansky, D. Levy, D. Esposito, L. Muthuswamy, A. Krasnitz, W. R. McCombie, J. Hicks and M. Wigler, Tumour evolution inferred by single-cell sequencing, *Nature*, 2011, **472**, 90–94.

57 S. M. Tu, M. A. Bilen and S. H. Lin, Radium-223: Optimizing Treatment and Research of Osteoblastic Bone Metastasis, *Oncology*, 2015, **29**, 490–492.

58 S. A. Amundson, K. T. Do, L. C. Vinikoor, R. A. Lee, C. A. Koch-Paiz, J. Ahn, M. Reimers, Y. Chen, D. A. Scudiero, J. N. Weinstein, J. M. Trent, M. L. Bittner, P. S. Meltzer and A. J. Fornace, Jr., Integrating global gene expression and radiation survival parameters across the 60 cell lines of the National Cancer Institute Anticancer Drug Screen, *Cancer Res.*, 2008, **68**, 415–424.

59 M. H. Tsai, J. A. Cook, G. V. Chandramouli, W. DeGraff, H. Yan, S. Zhao, C. N. Coleman, J. B. Mitchell and E. Y. Chuang, Gene expression profiling of breast, prostate, and glioma cells following single versus fractionated doses of radiation, *Cancer Res.*, 2007, **67**, 3845–3852.

60 R. D. Wood, M. Mitchell, J. Sgouros and T. Lindahl, Human DNA repair genes, *Science*, 2001, **291**, 1284–1289.

61 Z. C. Fu, F. M. Wang and J. M. Cai, Gene expression changes in residual advanced cervical cancer after radiotherapy: indicators of poor prognosis and radioresistance?, *Med. Sci. Monit.*, 2015, **21**, 1276–1287.

62 A. Helland, H. Johnsen, C. Froyland, H. B. Landmark, A. B. Saetersdal, M. M. Holmen, T. Gjertsen, J. M. Nesland, W. Ottestad, S. S. Jeffrey, L. O. Ottestad, O. K. Rodningen, G. Sherlock and A. L. Borresen-Dale, Radiation-induced effects on gene expression: an in vivo study on breast cancer, *Radiother. Oncol.*, 2006, **80**, 230–235.

63 G. W. Birrell, J. A. Brown, H. I. Wu, G. Giaever, A. M. Chu, R. W. Davis and J. M. Brown, Transcriptional response of *Saccharomyces cerevisiae* to DNA-damaging agents does not identify the genes that protect against these agents, *Proc. Natl. Acad. Sci. U. S. A.*, 2002, **99**, 8778–8783.

64 M. J. Daly, A new perspective on radiation resistance based on Deinococcus radiodurans, *Nat. Rev. Microbiol.*, 2009, **7**, 237–245.

65 P. L. Ståhl, F. Salmén, S. Vickovic, A. Lundmark, J. F. Navarro, J. Magnusson, S. Giacomello, M. Asp, J. O. Westholm, M. Huss, A. Mollbrink, S. Linnarsson, S. Codeluppi, Å. Borg, F. Pontén, P. I. Costea, P. Sahlén, J. Mulder, O. Bergmann, J. Lundeberg and J. Frisén, Visualization and analysis of gene expression in tissue sections by spatial transcriptomics, *Science*, 2016, **353**, 78.

66 J. Mele, H. Van Remmen, J. Vijg and A. Richardson, Characterization of transgenic mice that overexpress both copper zinc superoxide dismutase and catalase, *Antioxid. Redox Signaling*, 2006, **8**, 628–638.

67 N. G. Westman and S. L. Marklund, Copper- and zinc-containing superoxide dismutase and manganese-containing superoxide dismutase in human tissues and human malignant tumors, *Cancer Res.*, 1981, **41**, 2962–2966.

68 V. L. Kinnula, T. Torkkeli, P. Kristo, R. Sormunen, Y. Soini, P. Paakko, T. Ollikainen, K. Kahlos, A. Hirvonen and S. Knuutila, Ultrastructural and chromosomal studies on manganese superoxide dismutase in malignant mesothelioma, *Am. J. Respir. Cell Mol. Biol.*, 2004, **31**, 147–153.

69 S. L. Marklund, N. G. Westman, E. Lundgren and G. Roos, Copper- and zinc-containing superoxide dismutase, manganese-containing superoxide dismutase, catalase, and glutathione peroxidase in normal and neoplastic human cell lines and normal human tissues, *Cancer Res.*, 1982, **42**, 1955–1961.

70 S. L. Marklund, N. G. Westman, G. Roos and J. Carlsson, Radiation resistance and the CuZn superoxide dismutase, Mn superoxide dismutase, catalase, and glutathione peroxidase activities of seven human cell lines, *Radiat. Res.*, 1984, **100**, 115–123.

71 J. Sun, Y. Chen, M. Li and Z. Ge, Role of antioxidant enzymes on ionizing radiation resistance, *Free Radical Biol. Med.*, 1998, **24**, 586–593.

72 A. Suresh, F. Tung, J. Moreb and J. R. Zucali, Role of manganese superoxide dismutase in radioprotection using gene transfer studies, *Cancer Gene Ther.*, 1994, **1**, 85–90.

73 J. Chung-man, Ho, S. Zheng, S. A. Comhair, C. Farver and S. C. Erzurum, Differential expression of manganese superoxide dismutase and catalase in lung cancer, *Cancer Res.*, 2001, **61**, 8578–8585.

74 A. M. Janssen, C. B. Bosman, C. F. Sier, G. Griffioen, F. J. Kubben, C. B. Lamers, J. H. van Krieken, C. J. van de Velde and H. W. Verspaget, Superoxide dismutases in relation to the overall survival of colorectal cancer patients, *Br. J. Cancer*, 1998, **78**, 1051–1057.

75 M. Landriscina, F. Remiddi, F. Ria, B. Palazzotti, M. E. De Leo, M. Iacoangeli, R. Rosselli, M. Scerrati and T. Galeotti, The level of MnSOD is directly correlated with grade of brain tumours of neuroepithelial origin, *Br. J. Cancer*, 1996, **74**, 1877–1885.

76 D. Kovala-Demertzi, D. Hadjipavlou-Litina, M. Staninska, A. Primikiri, C. Kotoglou and M. A. Demertzis, Anti-oxidant, *in vitro*, *in vivo* anti-inflammatory activity and antiproliferative activity of mefenamic acid and its metal complexes with manganese(II), cobalt(II), nickel(II), copper(II) and zinc(II), *J. Enzyme Inhib. Med. Chem.*, 2009, **24**, 742–752.

77 J. S. Haviland, J. R. Owen, J. A. Dewar, R. K. Agrawal, J. Barrett, P. J. Barrett-Lee, H. J. Dobbs, P. Hopwood, P. A. Lawton, B. J. Magee, J. Mills, S. Simmons, M. A. Sydenham, K. Venables, J. M. Bliss and J. R. Yarnold, The UK Standardisation of Breast Radiotherapy (START) trials of radiotherapy hypofractionation for treatment of early breast cancer: 10-year follow-up results of two randomised controlled trials, *Lancet Oncol.*, 2013, **14**, 1086–1094.

78 B. D. Smith, J. R. Bellon, R. Blitzblau, G. Freedman, B. Haffty, C. Hahn, F. Halberg, K. Hoffman, K. Horst, J. Moran, C. Patton, J. Perlmutter, L. Warren, T. Whelan, J. L. Wright and R. Jagsi, Radiation therapy for the whole breast: Executive summary of an American Society for Radiation Oncology (ASTRO) evidence-based guideline, *Pract. Radiat. Oncol.*, 2018, **8**, 145–152.

79 C. Giesen, H. A. O. Wang, D. Schapiro, N. Zivanovic, A. Jacobs, B. Hattendorf, P. J. Schüffler, D. Grolimund, J. M. Buhmann, S. Brandt, Z. Varga, P. J. Wild, D. Günther and B. Bodenmiller, Highly multiplexed imaging of tumor tissues with subcellular resolution by mass cytometry, *Nat. Methods*, 2014, **11**, 417.

80 B. Paul, D. J. Hare, D. P. Bishop, C. Paton, V. T. Nguyen, N. Cole, M. M. Niedwiecki, E. Andreozzi, A. Vais, J. L. Billings, L. Bray, A. I. Bush, G. McColl, B. R. Roberts, P. A. Adlard, D. I. Finkelstein, J. Hellstrom, J. M. Hergt, J. D. Woodhead and P. A. Doble, Visualising mouse neuroanatomy and function by metal distribution using laser ablation-inductively coupled plasma-mass spectrometry imaging, *Chem. Sci.*, 2015, **6**, 5383–5393.